AWARD NUMBER: W81XWH-12-1-0316

TITLE: Targeting phosphatidylserine for radioimmunotherapy of breast cancer brain metastasis

PRINCIPAL INVESTIGATOR: Rolf A. Brekken

CONTRACTING ORGANIZATION: University of Texas Southwestern Medical Center
Dallas, TX 75390-9105

REPORT DATE: October 2013

TYPE OF REPORT: Annual

PREPARED FOR: U.S. Army Medical Research and Materiel Command
Fort Detrick, Maryland 21702-5012

REPORT DOCUMENTATION PAGE

Form Approved[3]
OMB No. 0704-0188

1. REPORT DATE *(DD-MM-YYYY)*	2. REPORT TYPE	3. DATES COVERED *(From - To)*\
October 2013	Annual	30September2012-29September2013

4. TITLE AND SUBTITLE

Targeting phosphatidylserine for radioimmunotherapy of breast cancer brain metastasis

5a. CONTRACT NUMBER
W81XWH-12-1-0316

5b. GRANT NUMBER
W81XWH-12-1-0316

5c. PROGRAM ELEMENT NUMBER

6. AUTHOR(S)

Rolf A. Brekken
Rolf.brekken@utsouthwestern.edu

5d. PROJECT NUMBER

5e. TASK NUMBER

5f. WORK UNIT NUMBER

7. PERFORMING ORGANIZATION NAME(S) AND ADDRESS(ES)

University of Texas Southwestern Medical Center
5323 Harry Hines Blvd
Dallas, TX 75390-9058

8. PERFORMING ORGANIZATION REPORT NUMBER

9. SPONSORING / MONITORING AGENCY NAME(S) AND ADDRESS(ES)

U.S. Army Medical Research
And Materiel Command
Fort Detrick, Maryland
21702-5012

10. SPONSOR/MONITOR'S ACRONYM(S)

11. SPONSOR/MONITOR'S REPORT NUMBER(S)

12. DISTRIBUTION / AVAILABILITY STATEMENT
Approved for public release; distribution unlimited

13. SUPPLEMENTARY NOTES

14. ABSTRACT

Brain metastasis occurs in ~30% of metastatic breast cancer patients. The prognosis is extremely poor, with a median survival of 4-6 months even with aggressive treatment. Thus, there is an urgent need to develop new treatments that target brain metastases. Radioimmunotherapy (RIT) is a targeted therapy that uses radiolabeled antibodies against tumor-specific antigens to treat lymphoma patients. However, success of RIT in the therapy of solid tumors has generally been limited due to heterogeneous tumor expression of the target antigens and cross-reactivity with normal cells. In preliminary studies, we have demonstrated that phosphatidylserine (PS) is exposed exclusively on tumor vascular endothelium of brain metastases in mouse models. A novel PS-targeting antibody, PGN635, a fully human monoclonal antibody, was used to target exposed PS in the brain metastases. Our data show that PGN635 binds specifically to tumor vascular endothelial cells in multi-focal brain metastases throughout the whole mouse brain. Vascular endothelium in normal brain tissues is negative. Furthermore, pretreatment with 10Gy of whole brain radiation significantly increased PGN635 binding to tumor vascular endothelial cells and tumor cells by increasing their exposure of PS. Vasculature in irradiated normal brain remained negative for exposed PS.

15. SUBJECT TERMS

16. SECURITY CLASSIFICATION OF: unclassified			17. LIMITATION OF ABSTRACT	18. NUMBER OF PAGES	19a. NAME OF RESPONSIBLE PERSON
a. REPORT	b. ABSTRACT	c. THIS PAGE	unlimited	29	Rolf A. Brekken
unclassified	unclassified	unclassified			19b. TELEPHONE NUMBER *(include area code)* 214.648.5151

Standard Form 298 (Rev. 8-98)
Prescribed by ANSI Std. Z39.18

Table of Contents

Page

Rolf A. Brekken, Ph.D.
Associate Professor, Surgery & Pharmacology
Effie Marie Cain Scholar in
Angiogenesis Research

Hamon Center for Therapeutic Oncology Research
Division of Surgical Oncology

14 April 2014

U.S. Army Medical Research and Materiel Command

RE: YR 1 Progress report for BC112653P1, DOD award # W81XWH-12-1-0316

Dear Review Committee:

I want to apologize for the long delay in submitting the progress report for the above referenced project. We are very thankful that the DOD has provided funding for this important and exciting project. The delay was entirely my fault and should not reflect a lack of interest from my lab or the lab of our collaborator Dr. Dawen Zhao. I knew that Dr. Zhao had submitted a progress report and was mistaken when I thought that his progress report was sufficient for the reporting requirements. You notified me in January that I was delinquent and I failed to promptly respond accordingly, for this I apologize. I have attached the progress on the subsequent pages.

We are excited about the results thus far and believe that targeting phosphatidylserine (PS) is a very attractive strategy for enhancing the efficacy of radiotherapy for breast cancer brain metastasis. In part, this excitement is due to our recent improved understanding of the mechanism of antibody-mediated blockade of PS. PS is an immunosuppressive factor that functions as an upstream immune checkpoint. The biology is evolutionarily conserved and is hijacked by tumors and their metastases to facilitate tumor progression. We have recently published the first paper describing in detail the mechanism and how antibody-mediated blockade of PS stimulates antibody dependent cellular cytotoxicity, which is highly relevant to the breast cancer brain metastasis project.

Thank you for your consideration and I apologize for the delay.

Sincerely,

Rolf A. Brekken, PhD

UT Southwestern Medical Center 6000 Harry Hines Blvd. / Dallas, Texas 75390-8593 / (214)648-5151/ Fax (214)648-4940
E-Mail: rolf.brekken@utsouthwestern.edu

BC112653P1
Progress Report

Introduction

Brain metastasis is the most common intracranial malignancy in adults. The prognosis is extremely poor, with a median survival of 4-6 months even with treatment. Due to the high incidence of multiple lesions and limited leakage of most chemotherapeutic agents through blood brain barrier (BBB), the standard care for these patients involves whole brain radiotherapy (WBRT). WBRT is often associated with neurological complications that preclude delivery of the sufficient dose to tumor lesions. Radioimmunotherapy (RIT) using radiolabeled monoclonal antibodies against tumor-specific antigens offers the opportunity to selectively irradiate tumor cells while sparing normal tissues. We have recently applied a novel phosphatidylserine (PS)-targeting antibody, PGN635, a fully human monoclonal antibody to study brain metastases in mouse models of breast cancer. PS is an integral membrane phospholipid that is maintained on the inner leaflet of the plasma membrane. It becomes externalized under stressful conditions or when cells under programmed cell death. PS exposure is a conserved immunosuppressive signal that ser1ves as an immune checkpoint to prevent the induction of autoimmunity to dying cells. PGN635 and other antibodies developed by our group that target PS inhibit this immune checkpoint and stimulate a productive immune response to antibody coated cells. The overall goal of this proposal is to test the hypothesis that PS-targeted radioimmunotherapy provides an effective and safe treatment for brain metastases.

Prior work from the Thorpe laboratory has demonstrated that PS is externalized on vasculature in the tumor microenvironment (1). Importantly, therapy also increases the exposure of PS on endothelial cells and tumor cells and the localization of anti-PS antibodies to the tumor microenvironment. The anti-PS antibodies (e.g., PGN635) once bound block PS induced immune suppression and drive activation of an innate immune response against the tumor. This response includes antibody dependent cellular cytotoxicity (ADCC) which results in targeting of PS positive cells for immune mediated destruction. We have shown recently in murine models of prostate cancer that antibody mediated blockade of PS results in striking changes in immune cell phenotype and potent anti-tumor efficacy (2).

Results

The current proposal has 3 tasks.
Task 1. To study PS exposure on tumor vasculature and tumor cells of breast cancer brain metastasis and determine if exposed PS is increased by radiation.

Dr. Zhao's laboratory has established a model of brain metastasis where breast tumor cells (e.g., MDA-MB-231/BR cells) are seeded in the brain via intracardiac injection. His laboratory has also demonstrated that brian metastases established in this manner can be visualized via MRI. (Task 1; Parts a & b)

In collaboration with Dr. Zhao we have demonstrated that PS is exposed on the vasculature of breast cancer brain metastases and have evaluated microvessel density (MVD) and hypoxia. We are currently evaluating cellular proliferation and apoptosis via immunohistochemistry. (Task 1; Part c) See Figures below.

We have obtained tissue from mice bearing brain metastases that have been subjected to WBRT. These animals were injected iv with PGN635 4 hours prior to sacrifice. The tissue is being processed for immunohistochemical evaluation of PS exposure, MVD, markers of hypoxia, and cell proliferation and apoptosis. (Task 1; part d)

Task 2. To radiolabel mch635 and evaluate its biodistribution and pharmacokinetics in breast cancer brain metastasis.

We have produced and provided PGN635 F(ab')2 to Dr. Zhao who has provided an update on the imaging properties of the radiolabeled antibody fragment in his progress report.

Task 3. To evaluate radioimmunotherapy of breast cancer brain metastases. These studies are ongoing and will be completed in the time frame of the project.

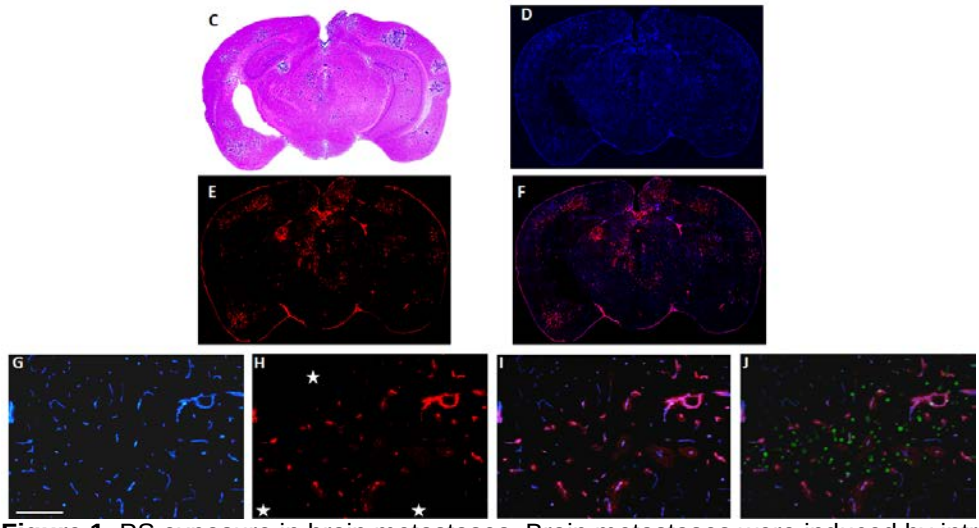

Figure 1. PS exposure in brain metastases. Brain metastases were induced by intracardiac injection of GFP – expressing MDA-MB-231/BR cells into immunocompromised mice. 5 weeks post tumor cell injection, animals were injected iv with PGN635, which binds to externalized PS, and mice were sacrificed 4 hrs post antibody injection. C) H&E histology of brain metastases. D-F) localization of PGN635 (**red,** E,F) to brain lesions counterstained with DAPI (**blue,** D, F). G-J) localization of PGN635 (**red,** H-J) with endothelial cell marker CD31 (**blue**, G, I). J) GFP detection (**green**) provides confirmation of tumor cells near PS+ blood vessels. K) quantification of the localization of PGN635 or a isotype control antibody (aurexis) to blood vessels in brain metastatic lesions.

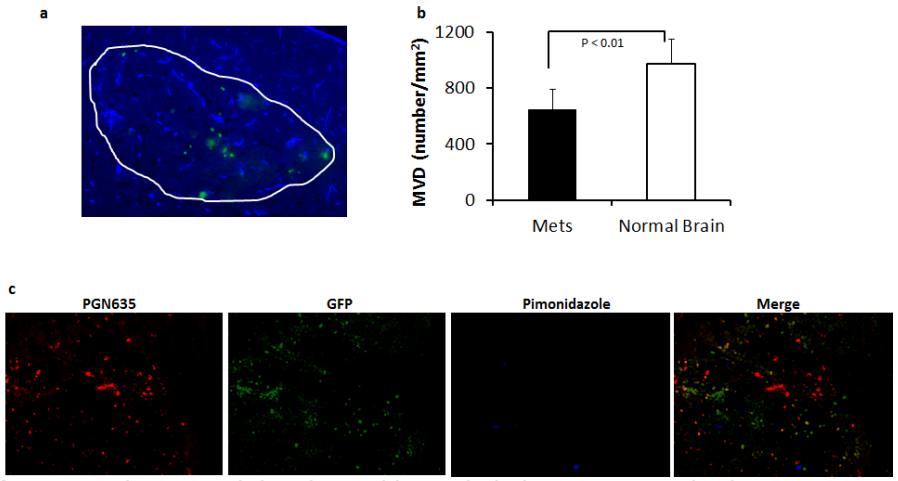

Figure 2. Microvessel density and hypoxia in breast cancer brain metastases. A,B) Sections of brain containing MDA-MB-231/BR-GFP metastases were evaluated for CD31+ blood vessels and compared to areas of normal non-involved brain. C) Localization of PGN635, tumor cells (GFP) and hypoxia (Pimonidazole) in brain metastases.

Key Research Accomplishments

• Establishment of the intracardiac model of breast cancer brain metastasis with various brain-tropic metastatic breast cancer cells including MDA-MB231Br-EGFR, MCF7Br-Her2 and syngeneic 4T1 cells.

• Successful application of longitudinal MRI to monitor intracranial metastases distribution, tumor growth and BTB permeability.

• Immunohistochemical studies show PS exposure is specifically located on tumor vascular endothelial cells of brain metastases while the normal vessels surrounding the metastases lack of exposed PS, suggesting that PS can serve as a brain metastasis specific biomarker.

• The fragments of PS-targeting antibody, PGN635F(ab')2 have been successfully conjugated with near infrared dye, allowing in vivo and ex vivo optical imaging of clear tumor contrast that enables demarcation of individual metastases from surrounding normal brain tissues.

• Immunohistochemical and histological studies of tumor vasculature, PS exposure and tumor hypoxia found no positive staining of tumor hypoxia marker, pimonidazole in individual metastases in the multifocal model of MDA-MB231Br-EGFP, excluding the possibility that tumor hypoxia induces PS exposure on tumor vascular endothelial cells.

• Autoradiography and PET imaging of radioactive iodine labeled PGN635 confirmed the targeting specificity of PGN635 and indicate the radiolabeled PGN635 can serve as a specific imaging probe for sensitive detection of brain metastases.

Challenges

The major challenge we have faced is the sudden passing of Dr. Thorpe. This caused a significant delay in making progress on the project. I have taken over the majority of the responsibilities that Dr. Thorpe had while also maintaining the projects I had running in my own independent laboratory. While our progress on this project has not been as rapid as anticipated, we have not slowed Dr. Zhao's progress on the project and we are confident that we will make rapid progress on the project.

Reportable outcomes

Recent PS related Publications:

Yin Y, Huang X, Lynn KD, Thorpe PE. Phosphatidylserine-targeting antibody induces M1 macrophage polarization and promotes myeloid-derived suppressor cell differentiation. *Can. Immunol. Res*. 2013. 1: 256-268.

Huang X and Brekken RA**.** Revitalizing tumor immunity by targeting PS. Science & Technology, published Dec 2103 http://www.paneuropeannetworks.com/ST9/#163/z

Stafford JH, Hao G, Best AM, Sun X, Thorpe PE. Highly specific PET imaging of prostate tumors in mice with an iodine-124-labeled antibody fragment that targets phosphatidylserine. *PLoS ONE* 2013. 8:e84864. PMID: 24367699.

Zhang L, Zhou H, Belzile O, Thorpe P, Zhao D. Phosphatidylserine-targeted bimodal liposomal nanoparticles for in vivo imaging of breast cancer in mice. *J. Controlled Release* 2014 epub ahead of print. PMID: 24698945.

Conclusion

During the first year of this project we have worked with Dr. Dawen Zhao to establish murine models of brain metastasis. Dr. Zhao has evaluated these models using MRI techniques that have enabled visualization of individual lesions in the brain. We have also exploited the specificity of PGN635, a human anti-PS antibody to visualize externalized PS on the vasculature and tumor cells in brain lesions. PGN635 specifically localized to the vasculature in metastases and did not react with blood vessels in normal brain tissue. We conclude that PS, as expected is an excellent marker of tumor vasculature and anticipate that therapy studies combining radiation and anti-PS, which are ongoing will provide potent therapeutic efficacy.

References

1. He J, Yin Y, Luster TA, Watkins L, Thorpe PE. Antiphosphatidylserine antibody combined with irradiation damages blood vessels and induces tumor immunity in a rat model of glioblastoma. Clin. Can. Res. 2009 15: 6871-6880. PMID: 19887482.
2. Yin Y, Huang X, Lynn KD, Thorpe PE. Phosphatidylserine-targeting antibody induces M1 macrophage polarization and promotes myeloid-derived suppressor cell differentiation. *Can. Immunol. Res*. 2013. 1: 256-268.

Published OnlineFirst August 19, 2013; DOI: 10.1158/2326-6066.CIR-13-0073

Cancer Immunology Research

Phosphatidylserine-Targeting Antibody Induces M1 Macrophage Polarization and Promotes Myeloid-Derived Suppressor Cell Differentiation

Yi Yin, Xianming Huang, Kristi D. Lynn, et al.

Cancer Immunol Res Published OnlineFirst August 19, 2013.

Published OnlineFirst August 19, 2013; DOI: 10.1158/2326-6066.CIR-13-0073

Cancer Immunology Research

Research Article

Phosphatidylserine-Targeting Antibody Induces M1 Macrophage Polarization and Promotes Myeloid-Derived Suppressor Cell Differentiation

Yi Yin, Xianming Huang, Kristi D. Lynn, and Philip E. Thorpe

Abstract

Multiple tumor-derived factors are responsible for the accumulation and expansion of immune-suppressing myeloid-derived suppressor cells (MDSC) and M2-like tumor-associated macrophages (TAM) in tumors. Here, we show that treatment of tumor-bearing mice with docetaxel in combination with the phosphatidylserine-targeting antibody 2aG4 potently suppressed the growth and progression of prostate tumors, depleted M2-like TAMs, and MDSCs, and increased the presence of M1-like TAMs and mature dendritic cells in the tumors. In addition, the antibody markedly altered the cytokine balance in the tumor microenvironment from immunosuppressive to immunostimulatory. *In vitro* studies confirmed that 2aG4 repolarized TAMs from an M2- to an M1-like phenotype and drove the differentiation of MDSCs into M1-like TAMs and functional dendritic cells. These data suggest that phosphatidylserine is responsible for the expansion of MDSCs and M2-like TAMs in tumors, and that bavituximab, a phosphatidylserine-targeting antibody currently in clinical trials for cancer, could reverse this process and reactivate antitumor immunity. *Cancer Immunol Res; 1(4); 1–13. ©2013 AACR.*

Introduction

Tumors have long been recognized as having immunosuppressive microenvironments that thwart the host's ability to control tumor growth (1, 2). Myeloid progenitors from the bone marrow populate tumors and differentiate into a heterogeneous population of myeloid-derived suppressor cells (MDSC) that are immunosuppressive (2). MDSCs secrete immunosuppressive cytokines, including interleukin (IL)-10 and TGF-β, that induce the development of regulatory T cells (Treg; refs. 3, 4), suppress immune responses mediated by $CD4^+$ and $CD8^+$ T cells (5–7), and the cytotoxic activities of natural killer (NK) and NKT cells (8). MDSCs of monocytic subtype ($CD11b^+$, $Gr\text{-}1^+$, and $Ly\text{-}6C^{Hi}$) differentiate into tumor-associated macrophages (TAM) and dendritic cells with impaired functionality (9–11). Dendritic cells remain immature and lack the costimulatory molecules needed to function as antigen-presenting cells (APC; ref. 12). TAMs become predominantly polarized into the alternatively activated M2-like phenotype that secrete proangiogenic factors (13) and immunosuppressive cytokines that further limit T-helper 1 immune responses (14). In contrast, classically activated M1-like TAMs secrete immunostimulatory cytokines that have direct tumoricidal activity. M1-like TAMs, however, are sparse and confined to the less hypoxic regions of tumors (15). The presence of M2-like TAMs in tumors correlates with poor prognosis (16, 17), whereas the presence of M1-like TAMs correlates with longer survival for patients (18).

Phosphatidylserine is a phospholipid that contributes to the immunosuppressed tumor microenvironment by preventing immune and inflammatory reactions (19–21). Phosphatidylserine is confined to the inner leaflet of the plasma membrane in most normal mammalian cells but becomes exposed on the outer surface of apoptotic cells, where it subverts unwanted immune reactions against dying cells (22). Antitumor responses are similarly suppressed in the tumor microenvironment because phosphatidylserine is exposed on endothelial cells in the tumor vasculature (23, 24) and on tumor-derived microvesicles (25); phosphatidylserine is expressed constitutively on some tumor cells (26). Moreover, the exposure of phosphatidylserine is increased significantly on tumor cells undergoing apoptosis in response to chemo- and radiotherapy, where it further enhances immunosuppression (27, 28). Exposed phosphatidylserine is recognized by macrophages and dendritic cells, which have receptors that recognize phosphatidylserine directly through TIM 3 and TIM 4, brain-specific

Authors' Affiliation: Department of Pharmacology and Simmons and Hamon Cancer Centers, University of Texas Southwestern Medical Center, Dallas, Texas

Note: Supplementary data for this article are available at Cancer Immunology Research Online (http://cancerimmunolres.aacrjournals.org/).

Y. Yin and X. Huang contributed equally to this work.

The authors dedicate this work to the life and career of their beloved friend and mentor, P.E. Thorpe.

Corresponding Author: Xianming Huang, Department of Pharmacology and Simmons and Hamon Cancer Centers, University of Texas Southwestern Medical Center, 2201 Inwood Road NC7.304, Dallas, TX 75390-8594. Phone: 214-648-1623; Fax: 214-648-1613; E-mail: xianming.huang@UTSouthwestern.edu

doi: 10.1158/2326-6066.CIR-13-0073

Published OnlineFirst August 19, 2013; DOI: 10.1158/2326-6066.CIR-13-0073

angiogenesis inhibitor 1 (BAI1), stabilin-2, or receptor for advanced glycation end-products (RAGE; refs. 29–32), or indirectly through a variety of bridging proteins (33, 34). Binding to macrophage phosphatidylserine receptors triggers IL-10- and TGF-β–dependent immunosuppressive signals that stimulate them to engulf the phosphatidylserine-expressing cells without secreting inflammatory cytokines (19–21). Moreover, while intratumoral dendritic cells bind and ingest phosphatidylserine-expressing cells, they maintain an immature phenotype, lacking the costimulatory molecules required for APC activity (35, 36). These data emphasize that exposed phosphatidylserine is a major factor in maintaining the immunosuppressed state in tumors, and further suggest that chemotherapy, radiotherapy, and androgen-deprivation therapy are undermined by the phosphatidylserine in the tumor microenvironment (37).

To explore the possibility of reversing the immunosuppressive effects of exposed phosphatidylserine, we generated a family of phosphatidylserine-targeting antibodies that bind with high affinity to complexes of the phosphatidylserine-binding plasma protein, β2-glycoprotein I (β2GP1) and anionic phospholipids. The antibodies bind to phosphatidylserine-expressing membranes by cross-linking two molecules of β2GP1 bound to phosphatidylserine on the membrane. The antibody–β2GP1–PS complex is only stably formed on phosphatidylserine-containing surfaces. 2aG4, a mouse immunoglobulin G2a (IgG2a) version of the human chimeric antibody bavituximab, localizes to phosphatidylserine-expressing tumor vascular endothelium and elicits strong antitumor effects when combined with chemo- or radiotherapy in mouse tumor models (24, 27, 28). Bavituximab is currently being tested in multiple clinical trials (38–40). Despite the progress that has been made, the mechanism of action of anti-phosphatidylserine antibodies is not fully understood.

In this study, we examined whether 2aG4 can reverse the immunosuppressive effects of exposed phosphatidylserine in mouse models of human prostate cancer. We show that 2aG4 reactivates antitumor immunity on multiple levels: (i) the switching of TAMs to a tumoricidal M1-like phenotype; (ii) the reduction of MDSCs in tumors; and (iii) the maturation of dendritic cells into functional APCs. Our data show that the antitumor activity of bavituximab is due in large part to the suppression of immune tolerance and a concomitant reactivation of antitumor immunity, generating M1-TAMs that destroy phosphatidylserine-expressing tumor vasculature.

Materials and Methods

Cell lines

Human prostate cancer cell lines LNCaP and PC3, and the C44 hybridoma (CRL-1943) were obtained from the American Type Culture Collection. PC3 cells were stably transfected with firefly luciferase (Jer-Tsong Hsieh, University of Texas Southwestern Medical Center, Dallas, TX). These cell lines were maintained in RPMI-1640 supplemented with 10% v/v heat-inactivated FBS (Hyclone) without antibiotics. All cell lines were regularly tested for *Mycoplasma*.

Antibodies

2aG4 (mouse IgG2a), C44 (control mouse IgG2a), and bavituximab (mouse 2aG4 VH and Vκ, human IgG1 κ constant domains) were produced by Peregrine Pharmaceuticals, Inc. Human β2GP1 was purified as previously described (41). All were endotoxin-free. Rituximab was from Genentech. Rat anti-mouse CD31, rat anti-mouse CD11b (M1/70, Mac-1), rat anti-mouse F4/80, rat anti-mouse Ly-6G (Gr-1), hamster anti-mouse CD11c (integrin αM-chain), hamster anti-mouse CD80, rat anti-mouse FcγIII/II receptor (CD16/CD32) monoclonal antibodies, and rabbit anti-mouse inducible nitric oxide (NO) synthase (iNOS) polyclonal antibody were from BD Pharmingen. Rat anti-mouse CD49b and rat anti-mouse NKG2A/C/E monoclonal antibodies were from Serotec Inc. Goat anti-mouse arginase-I (Arg-1) polyclonal antibody was from Santa Cruz Biotechnology, Inc. Hamster anti-mouse CD31 was from Pierce Biotechnology. All secondary antibodies for immunohistochemistry were from Jackson ImmunoResearch Labs. Fluorescein isothiocyanate (FITC)- or phycoerythrin (PE)-conjugated anti-CD11b (clone M1/70), FITC- or PE-conjugated anti-F4/80, FITC-conjugated anti-Ly6C (clone ER-MP20), allophycocyanin-conjugated anti-Gr-1 (clone RB6-8C5), and FITC- or PE-conjugated normal hamster IgG and rat IgG were from eBiosciences.

Animals

Male severe combined immunodeficient mice (SCID; NCI-ncr) mice 5 to 6 weeks old were purchased from the National Cancer Institute-Frederick Cancer Research Facility (Frederick, MD). All experimental procedures were approved by the University of Texas Southwestern's Animal Care and Use Committee.

Tumor studies

Prostate cancer PC3 and LNCaP tumors were selected for the study because almost all TAMs are of the M2-like phenotype, and have few transitioning cells, which makes them good tumor models in which to show M2 to M1 polarization.

Subcutaneous injections. Tumor cells (1×10^6 cells/0.1 mL/mouse) suspended in 50% Matrigel in PBS were injected s.c. into the right flank of male SCID mice. Tumor volumes were calculated as $V = (a^2 \times b)/2$, where a and b were the minimal and maximal diameters of the tumor, respectively.

Orthotopic injection. Male mice were anesthetized and PC3 cells (5×10^5 cells in 50 μL PBS) were injected into the dorsolateral prostate lobes after surgical exposure of the prostate. Bioluminescence imaging (BLI) was carried out while mice were under anesthesia.

Growth-inhibition studies. When LNCaP tumors reached 0.8 to 1.0 cm diameter or when BLI signals for orthotopic PC3 tumors reached 1×10^6 photons/s (equivalent to 20 mm^3), mice were randomized into groups and treated intraperitoneally (i.p.) twice weekly with C44, 2aG4 (4 mg/kg), docetaxel (5 mg/kg), or a combination of both 2aG4 and docetaxel. Because the binding of bavituximab and 2aG4 to phosphatidylserine is dependent on human β2GP1, antibodies were coadministered with β2GP1 (4 mg/kg) in all experiments.

Published OnlineFirst August 19, 2013; DOI: 10.1158/2326-6066.CIR-13-0073

Bioluminescence imaging

BLI was conducted on the IVIS200 system with the use of Living Image acquisition and analysis software (Caliper Life Sciences). Luciferin (75 mg/kg; Biosynth Chemistry & Biology) was injected s.c., and serial 5-second images were acquired between 5 and 10 minutes after injections. Signal intensity was quantified as the sum of all detected photon counts within a manually selected region of interest that was kept constant at each time point.

Quantification of tumor endothelium with exposed phosphatidylserine

Mice bearing s.c. PC3 or LNCaP tumors of 1 cm in diameter were injected i.v. with 100 μg of bavituximab or rituximab; after 2 hours, these mice were anesthetized and perfused with heparinized saline. Major organs and tumors were removed and snap-frozen, and 8-μm sections were generated from the center of the tumors. Bavituximab-positive vessels were identified with biotinylated goat anti-human IgG followed by Cy2-labeled streptavidin (green). Vascular endothelium was identified with rat anti-mouse CD31 antibody followed by Cy3-labeled goat anti-rat IgG (red). Sections were counterstained with 4′,6′diamidino-2-phenylindole (DAPI) and assessed by fluorescence microscopy. Single images were captured using a Coolsnap digital camera and analyzed with ImageJ Version 1.44s software (Wayne Rasband, NIH) to quantify pixels positive for both CD31 and bavituximab. Five randomly selected 0.079-mm^2 fields were analyzed per section, with three sections per tumor and four to five tumors per group.

Blood vessel perfusion analysis

To quantify perfusible tumor vessels in mice, Hoechst 33342 (Sigma-Aldrich) was injected (15 mg/kg) into a tail vein, and 2 minutes later, mice were sacrificed and the tumors were removed and cryosectioned. Ten sections per tumor and five tumors per group were analyzed and perfusion measured over the entire tumor section. The mean percentage of the area of tumor sections that was stained with Hoeschst 33342 dye was quantified using the ImageJ software.

Blood flow quantification

Tumors were sonographically scanned with a Vevo 770 small-animal high-resolution ultrasound scanner equipped with a VisualSonics RMV 708 scan head (VisualSonics). Three-dimensional (3D) images in power Doppler mode were obtained by acquiring two-dimensional (2D) images every 100 μm along the entire length of the tumor. Ultrasound scanner settings were power Doppler transmission frequency, 23 MHz; power gain, 100%, wall filter, 2.5 mm/s; and scan speed, 2.0 mm/s. The percentage of the tumor volume having detectable blood flow was computed using the 3D segmentation tool in the Vevo 770 software package.

Quantification of immune cells in tumor sections

Frozen sections (three sections/tumor; three to five tumors/group) were cut through the tumors at the widest dimension. The sections were stained with antibodies to identify various cell types: TAMs ($F4/80^+$), M1-subtype TAMs ($iNOS^+$ and $F4/80^+$), M2-subtype TAMs ($Arg\text{-}1^+$ and $F4/80^+$), NK cells ($NKG2A/CE^+$ and $CD49b^+$), MDSCs ($Gr\text{-}1^+$ and $CD11b^+$), transitioning MDSCs ($F4/80^+$ and $Gr\text{-}1^+$), granulocytes ($Gr\text{-}1^+$, $Ly6G^{hi}$, and $CD11b^-$), dendritic cells ($CD11b^+$ and $CD11c^{hi}$), and mature dendritic cells ($CD11c^{hi}$ and $CD86^+$). Double and triple staining were carried out with primary antibodies from different species and developed with appropriate Cy2-, Cy3-, or coumarin aminomethylcoumarin acetate–labeled anti-IgG secondary antibodies. The sections were counterstained with DAPI and analyzed by fluorescence microscopy. Digital images (five per section) were collected. For individual colors, the same exposure times and illumination intensity were used for different sections, and the data were collected and processed in the same way to ensure comparability. The area of double-stained cells was computed using ImageJ software and expressed as a mean percentage of the total area of the sections.

Real-time quantitative reverse transcription analyses

Expression levels of mRNA were quantified relative to housekeeping gene 18S rRNA (forward: GCAATTATTCCCCATGAACG; reverse: AGGGCCTCACTAAACCATCC). Gene-specific primers were used to detect the following: iNOS (forward: TTCTGTGCTGTCCCAGTGAG; reverse: TGAAGAAAACCCCTTGTGCT), Arg-1 (forward: AGAGATTATCGGAGCGCCTT; reverse: TTTTTCCAGCAGACCAGCTT), IL-6 (forward: TGATGCACTTGCAGAAAACA; reverse: ACCAGAGGAAATTTTCAATAGGC), IL-12 p40 (forward: AGCAGTAGCAGTTCCCCTGA; reverse: AGTCCCTTTGGTCCAGTGTG), CD206 (forward: GGCAGGATCTTGGCAACCTAGTA; reverse: GTTTGGATCGGCACACAAAGTC), IL-10 (forward: ATCGATTTCTCCCCTGTGAA; reverse: TGTCAAATTCATTCATGGCCT), TNF-α (forward: CCACCACGCTCTTCTGTCTAC; reverse: AGGGTCTGGGCCATAGAACT), TGF-β1 (forward: GGAGAGCCCTGGATACCAAC; reverse: CAACCCAGGTCCTTCCTAAA), Fizz-1 (forward: CCCTTCTCATCTGCATCTCC; reverse: CTGGATTGGCAAGAAGTTCC), Ym1 (forward: TCTGGGTACAAGATCCCTGAA; reverse: TTTCTCCAGTGTAGCCATCCTT), F4/80 (forward: TTACGATGGAATTCTCCTTGTATATCA; reverse: CACAGCAGGAAGGTGGCTATG), CD11c (forward: CTG GATAGCCTTTCTTCTGCTG; reverse: GCACACTGTGTCCGAACTCA), CD40 (forward: GTTTAAAGTCCCGGATGCGA; reverse: CTCAAGGCTATGCTGTCTGT), CD80 (forward: ACCCCCAACATAACTGAGTCT; reverse: TTCCAACCAAGAGAAGCGAGG), CD83 (forward: CGCAGCTCTCCTATGCAGTG; reverse: GTGTTTTGGATCGTCAGGGAATA), CD86 (forward: TGTTTCCGTGGAGACGCAAG; reverse: CAGCTCACTCAGGCTTATGTTTT), VEGF-A (forward: TTTACTGCTGTACCTCCACCA; reverse: ATCTCTCCTATGTGCTGGCTTT), VEGF-B (forward: CCTGGAAGAACACAGCCAAT; reverse: GGAGTGGGA TGGATGATGTC); MHC II (forward: GCGACGTGGGCGAGTACC; reverse: CATTCCGGAACCAGCGCA), Ccl 5 (forward: TGCCCACGTCAAGGAGTATTTC; reverse: AACCCACTTCTTCTCTGGGTTG), and Cxcl11 (forward: GGCTGCGACAAAGTTGAAGTGA; reverse: TCCTGGCACAGAGTTCTTATTGGAG).

Published OnlineFirst August 19, 2013; DOI: 10.1158/2326-6066.CIR-13-0073

Isolation of TAMs and monocytic MDSCs

For TAMs, tumors were minced into small pieces and incubated for 15 minutes at 37°C with collagenase type II (0.5 mg/mL), collagenase type IV (0.5 mg/mL), and DNase I (0.01 mg/mL). Tumor pieces were mechanically dissociated using a gentleMACS dissociator (Miltenyi Biotec Inc.). The dissociated cells were collected, red blood cells (RBC) were lysed, and 2.5×10^8 cells were transferred into tissue culture flasks. After 2 hours at 37°C, nonadherent and loosely adherent cells were washed away. The adherent cells were detached with Accutase, and TAMs were extracted using anti-F4/80–biotin followed by anti-biotin magnetic beads (Miltenyi Biotec, Inc.). TAMs were 95% $F4/80^+$ by fluorescence-activated cell sorting (FACS) analysis. Monocytic MDSCs were isolated from single-cell suspensions of spleen cells from tumor-bearing mice, by positive selection with anti-CD11b–coated magnetic beads, negative selection with anti-Ly6G-biotin followed by anti-biotin magnetic beads, and a final positive selection with anti-Gr-1–coated beads (Miltenyi Biotec, Inc.). Ninety percent of the cells were $CD11b^+$, $Ly6G^{lo}$, and $Ly6C^{hi}$ by FACS analysis.

Electron microscopy

Freshly isolated TAMs and MDSCs were lightly fixed for 5 minutes in 1% methanol-free formaldehyde (Polysciences, Inc.) in PBS. Cells were stained with both 2aG4 and rabbit anti-Alix (H-270; Santa Cruz Biotechnology, Inc.), or irrelevant control antibodies, followed by 12-nm gold-labeled donkey anti-mouse IgG and 6-nm gold-labeled donkey anti-rabbit IgG. Cells were processed for transmission electron microscopy (TEM) using standard methods. Ultrathin sections were viewed on a TEM Tecnai electron microscope.

Results

Inhibition of prostate cancer growth in mice

Combining 2aG4 with docetaxel treatment improved the therapeutic activity on prostate tumors in mice beyond that achievable with either drug alone. Both castration-resistant (PC3) and castration-sensitive (LNCaP) tumors responded to the combination treatment. Treatment of mice bearing established orthotopic PC3 tumors with the combination reduced the bioluminescence intensity of the tumors by 42-fold as compared with mice treated with the C44 control antibody (Fig. 1A and B). 2aG4 alone and docetaxel alone reduced the bioluminescence intensity by approximately 3- and 7-fold, respectively. These differences were confirmed by the weights of the genitourinary tract plus tumor at the end of the experiment (Fig. 1C). The combination treatment was not more toxic to mice than treatment with docetaxel alone; animals in both groups lost 15% more body weight than did the C44-treated controls (Fig. 1D). Physical signs were the same in both groups. 2aG4 treatment alone was not toxic.

The combined regimen of 2aG4 and docetaxel inhibited the growth of LNCaP tumors in mice to a similar extent. When combined with castration, the triple combination caused major regressions of large established tumors and prevented progression to castration-resistant disease (Supplementary Fig. S1A and S1B).

Exposure of phosphatidylserine on tumor blood vessels and amplification by docetaxel

In untreated mice, 22% and 21% of tumor vessels had exposed phosphatidylserine in the PC3 (Fig. 2A) and LNCaP tumors, respectively (Supplementary Fig. S2A). We have previously shown that phosphatidylserine-positive tumor endothelial cells seem to be viable: They lack cytoplasmic and nuclear markers of apoptosis, are morphologically intact, and the vessels transport solutes and blood (42). The percentage of phosphatidylserine-positive tumor vessels was increased markedly 48 hours after administration of a single dose of docetaxel with peak levels of 61% in PC3 tumors (Fig. 2A) and 56% in LNCaP tumors (Supplementary Fig. S2A). No staining was detected with an isotype-matched control antibody, rituximab. Blood vessels in normal tissues (brain, heart, small intestine, large intestine, leg muscle, liver, lung, kidney, and testis) remained phosphatidylserine-negative irrespective of docetaxel treatment. Except for cells in and around necrotic regions, tumor cells were phosphatidylserine-negative in animals not injected with docetaxel. After treatment with docetaxel, 15% to 30% of the tumor cells became phosphatidylserine-positive (data not shown).

Destruction of tumor vasculature by 2aG4

Treatment with 2aG4 caused vessels in PC3 tumors (Fig. 2B) and LNCaP tumors (Supplementary Fig. S2B) to become denuded of vascular endothelium. Collagen IV in the surrounding basement membrane remained, but there were no endothelial cells. Blood vessels in tumors from C44-treated mice were intact. Vascular damage was also evident from the reductions in vascular density, perfusion, and blood flow in PC3 and LNCaP tumors of mice treated with 2aG4 alone or in combination with docetaxel. After 2 weeks of treatment, the combination regimen reduced vascular density in PC3 tumors by 88% (Fig. 2C) and in LNCaP tumors by 84% (Supplementary Fig. S2C), whereas 2aG4 alone reduced vascular density in PC3 tumors by 51% and in LNCaP tumors by 60%, relative to C44 control groups ($P < 0.001$). Docetaxel alone had little effect on vascular density. Perfusion studies with the fluorescent DNA-binding dye, Hoechst 33342, showed that treatment with 2aG4 alone reduced the mean area of PC3 tumor sections occupied by the dye from 16% (C44 control group) to 8.5% and, in combination with docetaxel, to 2.5% (Fig. 2C). Similar reductions in perfusion were observed in LNCaP tumors (Supplementary Fig. S2C). Using Doppler 3D ultrasound measurements, we showed that the volume of PC3 tumors with detectable blood flow was reduced by 2aG4 treatment from 3.8% to 1.7% ($P < 0.0001$) and, when combined with docetaxel, to 0.8% (Fig. 2D).

Vascular damage is caused by M1-like TAMs generated by 2aG4 treatment

Immunohistochemical analyses of PC3 and LNCaP tumors from mice treated with 2aG4 alone or in combination with docetaxel revealed that vascular damage was caused by TAMs ($F4/80^+$, green) that congregated around $CD31^+$ tumor blood

Published OnlineFirst August 19, 2013; DOI: 10.1158/2326-6066.CIR-13-0073

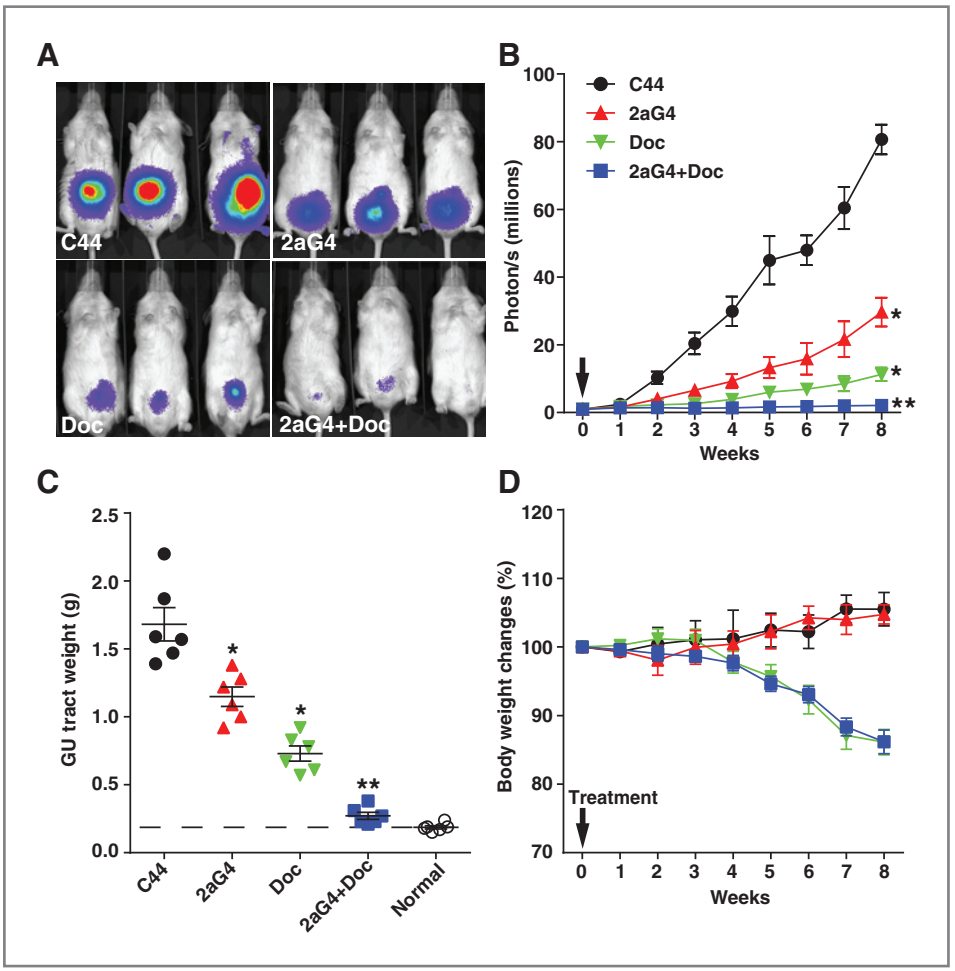

Figure 1. Inhibition of growth of orthotopic PC3 tumors in mice treated with 2aG4 alone or in combination with docetaxel. SCID mice (6 per group) bearing established orthotopic PC3 tumors were treated twice a week i.p. with C44 (black ●), 2aG4 (4 mg/kg; red ▲), docetaxel (5 mg/kg; green ▼), or 2aG4 plus docetaxel (blue ■). A, BLI of representative mice after 8 weeks of treatment. B, BLI measurements showing that 2aG4 retards tumor growth, particularly when given in combination with docetaxel. Points, mean; bars, ± SEM. *, Significant for 2aG4 or docetaxel versus C44 ($P < 0.0001$); **, significant for combination versus 2aG4 or docetaxel alone ($P < 0.02$; ANOVA followed by Tukey range test). C, genitourinary (GU) tract weights at sacrifice confirming tumor growth inhibition by 2aG4 and its enhancement by docetaxel. Weights above the normal genitourinary weight (dashed line) are assumed to be due to the tumor. Points, individual animals; horizontal lines, mean; bars, ± SD. *, Significant for 2aG4 or docetaxel versus C44 ($P < 0.001$); **, significant for combination versus 2aG4 or docetaxel alone ($P < 0.001$; ANOVA followed by Tukey range test). D, body weight changes indicating that combination is no more toxic than is docetaxel alone. Points, mean; bars, ± SD. Data are representative of three separate experiments.

vessels (red; Fig. 3A; Supplementary Fig. S3A). Only $CD31^+$ remnants of most of the vessels remained. TAMs were the only cell type present around damaged tumor blood vessels; there were no NK cells, granulocytes, or transitioning MDSCs ($F4/80^+$ and $Gr\text{-}1^+$). Almost all TAMs were costained with F4/80 and iNOS, and they lacked Arg-1, indicating that they were of the M1-like phenotype (Fig. 3B and Supplementary Fig. S3A). In sharp contrast, in mice treated with C44 or docetaxel alone, TAMs were costained with F4/80 and Arg-1 but not iNOS, indicating they were predominantly of the M2-like phenotype (Fig. 3C and Supplementary Fig. S3B). The M2-like TAMs were less abundant and scattered throughout the tumor interstitium; they were not associated with the vessels. A small fraction of TAMs were of mixed phenotypes, most likely representing transition states between M2 and M1.

The shift in polarity of TAMs from being predominantly M2-like to predominantly M1-like was confirmed by quantifying the mean area of tumor sections that double-stained for markers of M1 ($F4/80^+$ and $iNOS^+$) and M2 ($F4/80^+$ and $Arg\text{-}1^+$) TAMs. In PC3 tumors treated with C44, the mean area of sections occupied by M2-like TAMs was 2.5%, as compared with 1.4% for M1-like TAMs (Fig. 3D). In contrast, in tumors treated with 2aG4, the mean area occupied by M1-like TAMs increased to 9.4%, whereas the area occupied by M2-like TAMs decreased slightly to 1.3%. The M1:M2 ratio increased from 0.55 to 7.0, an increase of 12.7-fold (Fig. 3D). Similar changes were observed for LNCaP tumors treated with 2aG4, in which the M1:M2 ratio increased 18-fold (Supplementary Fig. S3C). These changes were supported by quantitative reverse-transcription PCR (qRT-PCR) studies on

Published OnlineFirst August 19, 2013; DOI: 10.1158/2326-6066.CIR-13-0073

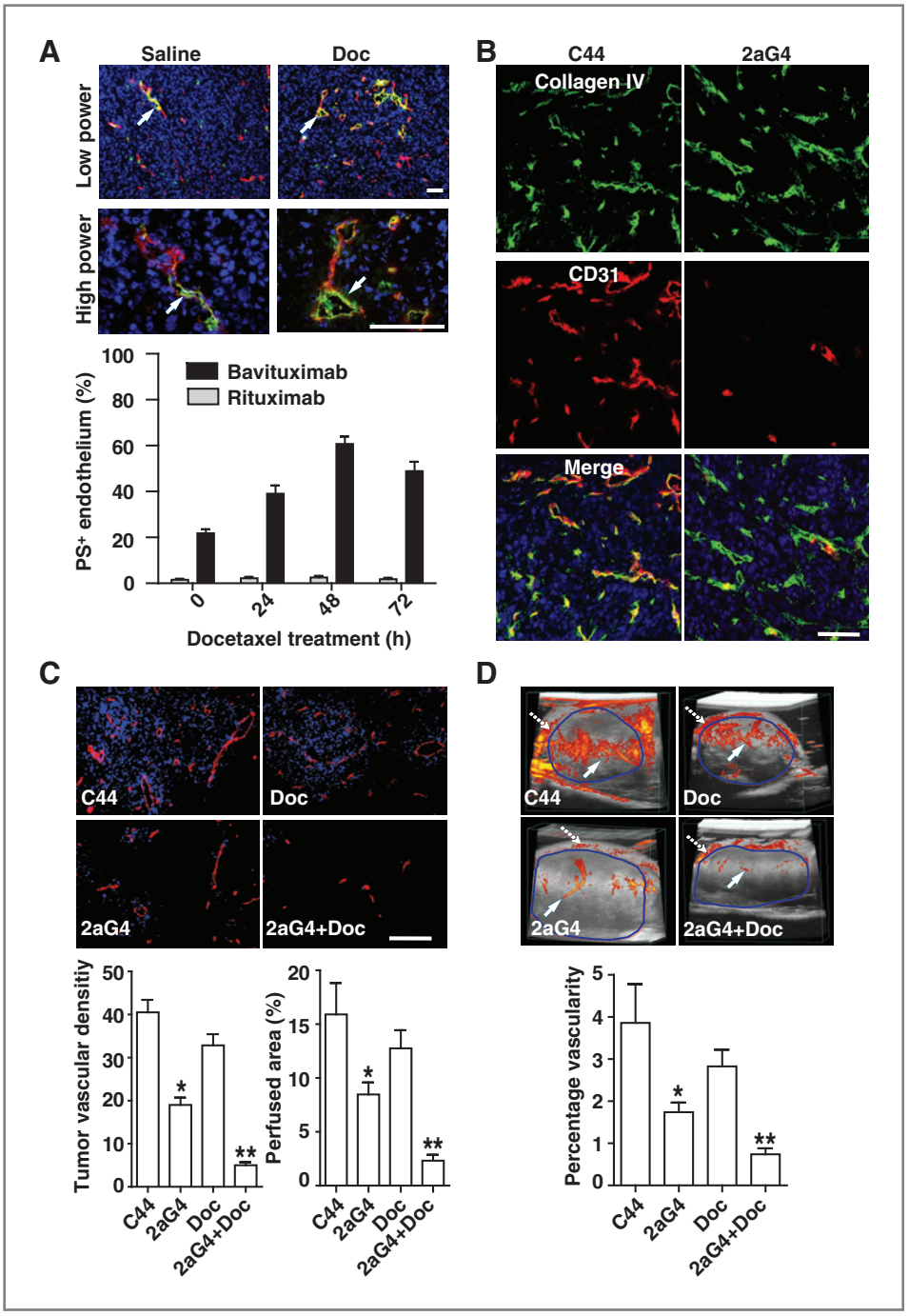

Figure 2. Damage to tumor vasculature induced by treatment with 2aG4. A, exposure of phosphatidylserine on tumor endothelium and amplification by docetaxel (Doc). Top, representative sections from PC3 tumor-bearing mice that had been injected with saline (left) or docetaxel (10 mg/kg, i.p, right) followed 48 hours later by bavituximab to detect phosphatidylserine or rituximab (control). Sections were stained for bavituximab (green), CD31 (red), and nuclei (DAPI; blue) and images merged. Arrows indicate bavituximab-stained vessels. The percentage of the $CD31^+$ area of sections that costained for phosphatidylserine reached a maximum 48 hours after injection of docetaxel (histograms). B, denudation of vascular endothelium in PC3 tumors in mice treated with 2aG4. The merged image (bottom right) shows stripped vessels, as identified by collagen IV staining (green) and absence of endothelium (CD31; red). C, reduction of tumor vascularity (vessels/0.079 mm^2) and perfusion (% area stained by Hoescht 33342 dye) in PC3 tumor-bearing mice treated with 2aG4 alone or in combination with docetaxel. D, 3D power Doppler ultrasound showing a reduction in blood flow in PC3 tumors in mice treated with 2aG4 alone or in combination with docetaxel. Tumor vessels, solid arrows; skin vessels, dotted arrows; outer margin of tumor, blue; histograms, percentage of tumor volume with detectable blood flow (percentage vascularity). In A, C, and D, 5 animals per group were analyzed. Histograms are mean ± SD. Number of determinations (n) were 120 to 150 in A, 50 in C, and 5 in D. *, Significant for 2aG4 versus C44 control ($P < 0.0001$); **, significant for 2aG4 plus docetaxel versus 2aG4 alone ($P < 0.0001$; Student two-tailed t test). Scale bars, 100 μm.

$F4/80^+$ TAMs isolated from dissociated PC3 tumors from 2aG4- or C44-treated mice. An increase in mRNA-encoding multiple M1 markers and a decrease in mRNA-encoding multiple M2 markers were observed after 2aG4 treatment (Fig. 3E). Among the increased M1 markers were the T-cell costimulatory molecules, CD80, CD86, CD40, and MHC class II, indicating that 2aG4 treatment caused the TAMs to acquire the ability to present antigens. Among the decreased M2 markers were VEGF-A and -B, indicating that 2aG4 treatment reduced the ability of TAMs to induce tumor angiogenesis. Treatment with 2aG4 also switched the production of cytokine mRNA from immunosuppressive (TGF-β and IL-10) to immunostimulatory (TNF-α and IL-12).

Next, we determined whether 2aG4 treatment could enhance NO production by TAMs and induce direct tumoricidal activity. TAMs isolated from 2aG4-treated PC3 tumors synthesized NO, whereas those from C44-treated tumors did not (Fig. 3F). TAMs from the 2aG4-treated tumors efficiently killed tumor cells *in vitro*, whereas those from C44-treated tumors did not (Fig. 3G). Thus, 2aG4 treatment generated tumoricidal M1-like TAMs.

Published OnlineFirst August 19, 2013; DOI: 10.1158/2326-6066.CIR-13-0073

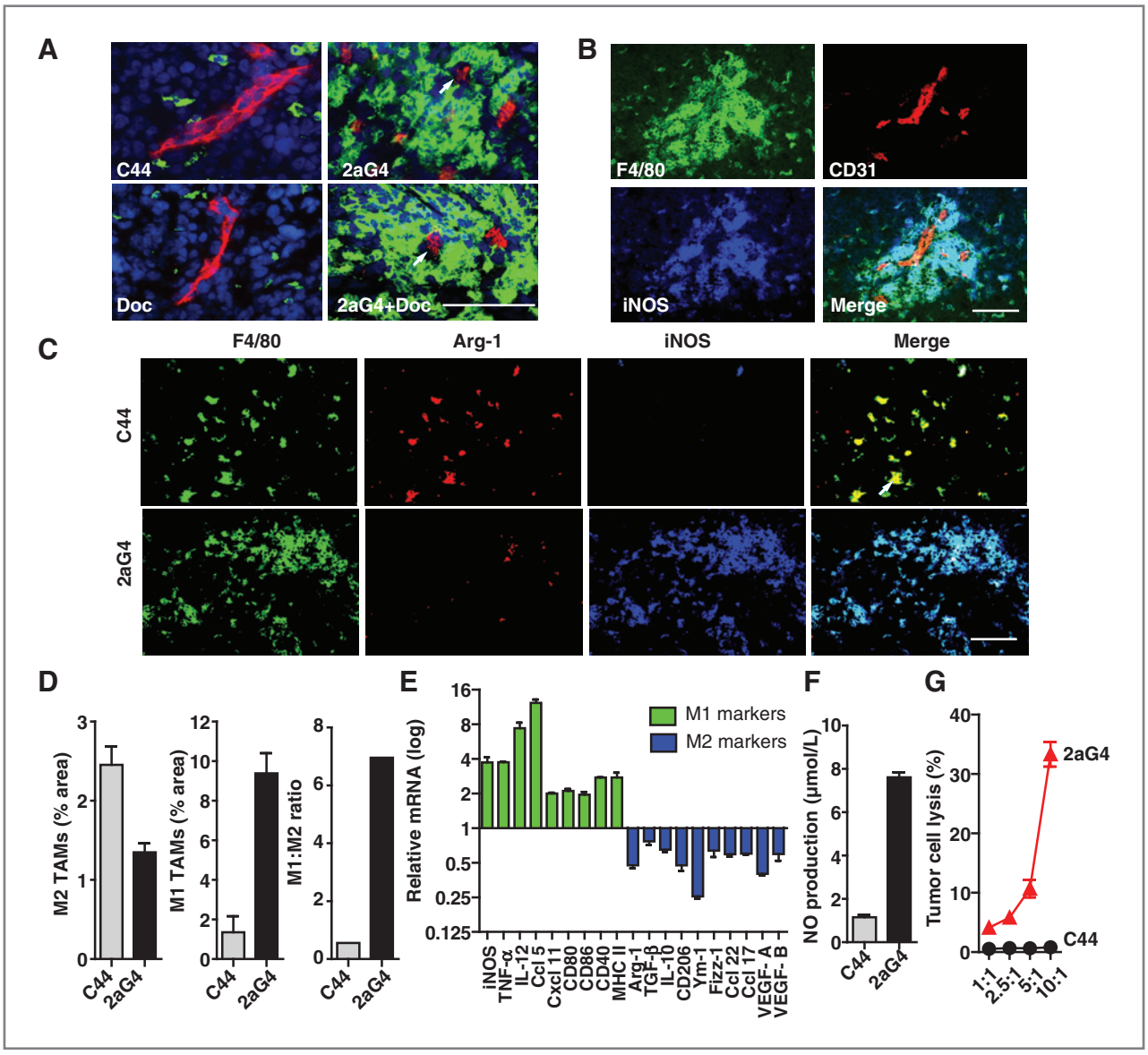

Figure 3. Vascular damage is caused by M1-like TAMs generated by 2aG4 treatment. A, representative frozen sections showing TAM-mediated disintegration of vascular endothelium in PC3 tumors from mice treated for 2 weeks with 2aG4, alone or in combination with docetaxel. Sections were stained to detect endothelial cells (CD31; red), TAMs (F4/80; green), and nuclei (DAPI; blue). Other cell types (NK, granulocytes, and dendritic cells) were not present in the packs of cells around damaged vessels (not shown). B, TAMs congregating around damaged vessels in 2aG4-treated mice costained for iNOS (blue) and F4/80 (green), indicating they were of M1-like phenotype. C, representative sections showing that 2aG4 treatment causes a shift in the predominant polarity of TAMs from M2-like (F4/80$^+$, green; Arg-1$^+$, red) in C44 mice (top) to M1-like (F4/80$^+$, green; iNOS$^+$, blue) in 2aG4-treated mice (bottom). D, a large increase in M1:M2 ratio in TAMs is caused by 2aG4 treatment. Histograms show the area of PC3 tumor sections occupied by M1 (F4/80$^+$ and iNOS$^+$) or M2 (F4/80$^+$ and Arg-1$^+$) TAMs, and the calculated M1:M2 ratio. E, qRT-PCR of RNA from purified tumor infiltrating F4/80$^+$ cells reveals a general increase in M1 markers and a decrease in M2 markers in tumors from 2aG4-treated mice relative to C44-treated mice. F, TAMs from 2aG4-treated mice manufacture NO (Griess assay). G, TAMs from 2aG4-treated mice are tumoricidal (^{51}Cr release assay). Horizontal axis, TAM:tumor cell ratio. Histograms are mean ± SD. Number of determinations (*n*) was 60 (4 mice/group; D) and 5 (C, F, and G). All differences between 2aG4 versus C44 control are statistically significant ($P < 0.0001$; Student two-tailed *t* test). Scale bars, 100 μm.

Treatment with 2aG4 decreases MDSCs, increases TAMs and mature dendritic cells, and shifts the balance of cytokines in the tumor microenvironment from immunosuppressive to immunostimulatory

Sections of PC3 or LNCaP tumors from 2aG4- or C44-treated mice were stained for MDSCs (CD11b$^+$ and Gr-1$^+$), TAMs (F4/80$^+$), and mature dendritic cells (CD11c^{hi} and CD86^{hi}). TAMs did not costain for Gr-1, indicating the absence of transitioning MDSCs. The mean area of tumor sections occupied by these cells was quantified and is shown together with representative sections in Fig. 4A and Supplementary Fig. S4A. Treatment of PC3 tumors

Published OnlineFirst August 19, 2013; DOI: 10.1158/2326-6066.CIR-13-0073

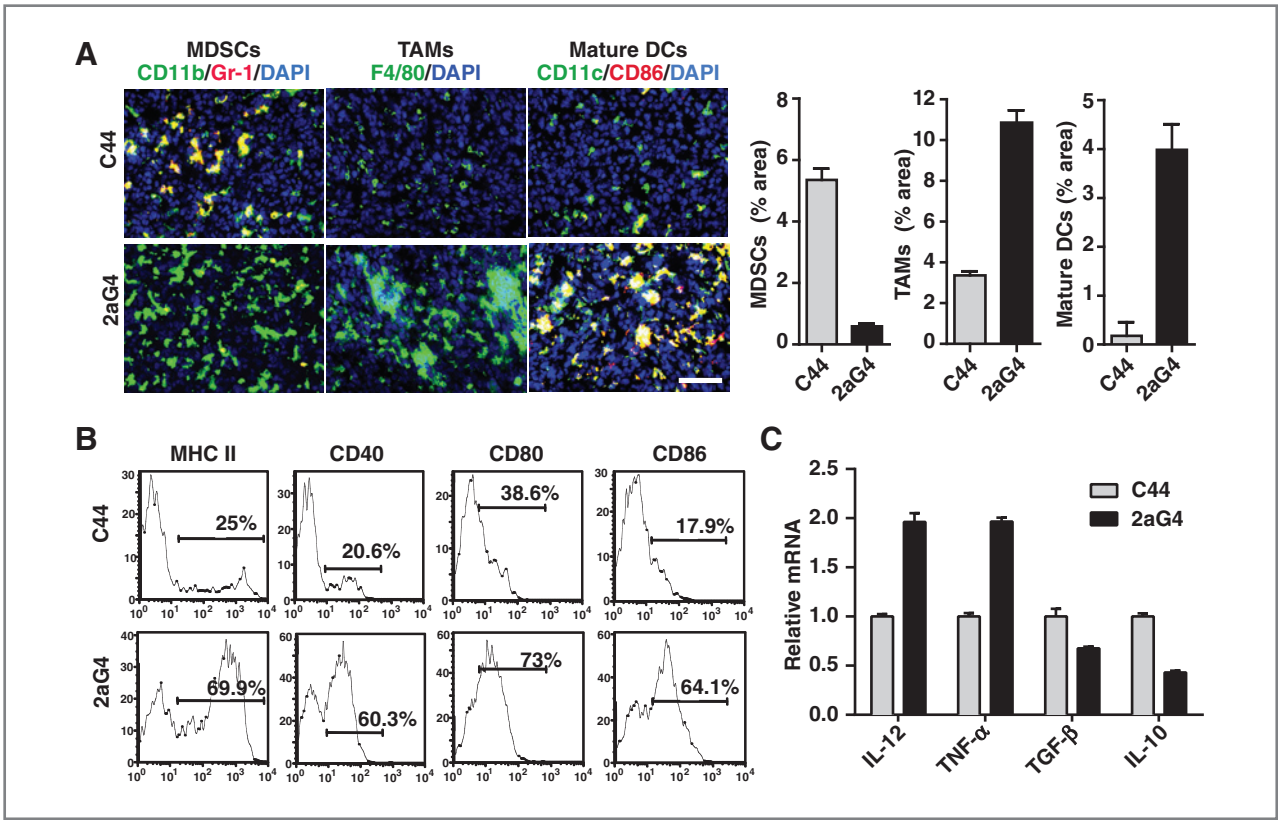

Figure 4. 2aG4 treatment of tumor-bearing mice decreases MDSCs, increases TAMs and mature dendritic cells (DC), and shifts the balance of cytokines in the tumor microenvironment from immunosuppressive to immunostimulatory. A, representative frozen sections of subcutaneous PC3 tumors showing that 2aG4 treatment of the mice decreases the presence of MDSCs and increases the presence of TAMs and mature dendritic cells. Top, control mice; bottom, 2aG4-treated mice. The sections were stained for MDSCs ($CD11b^+$ and $Gr\text{-}1^+$), TAMs ($F4/80^+$), mature dendritic cells ($CD11c^{hi}$ and $CD86^{hi}$), and nuclei (DAPI; blue). MDSCs (left) and mature dendritic cells (right) appear yellow in the merged images. TAMs in the central panels appear green. The histograms show the mean percentage area ± SD of tumor sections occupied by the cells. Differences between 2aG4 and C44 are significant ($P = 0.0002$; $n = 40$; Student two-tailed t test). Scale bar, 100 μm. B, 2aG4 treatment induces expression of T-cell costimulatory molecules on $CD11b^+$ cells in PC3 tumors. $CD11b^+$ cells were isolated from disaggregated tumors from mice treated with C44 (top) or 2aG4 (bottom) and analyzed by FACS. C, 2aG4 treatment of PC3 tumor-bearing mice increases production of immunostimulatory IL-12 and TNF-α in the tumor microenvironment and decreases the production of immunosuppressive TGF-β and IL-10. Homogenates of tumors from 2aG4- or C44-treated mice were analyzed for mouse cytokine mRNA by qRT-PCR. The histograms show the levels in 2aG4-treated tumors relative to the levels in C44-treated tumors (mean ± SD of triplicate measures; data representative of three separate experiments).

with 2aG4 decreased the mean area of tumor sections occupied by MDSCs by 8-fold, increased the mean area occupied by TAMs by 3-fold, and by mature dendritic cells by 23-fold (Fig. 4A; $P < 0.001$). Similar changes were observed for LNCaP tumors (Supplementary Fig. S4B). FACS analyses showed that 2aG4 treatment increased the percentage of $CD11b^+$ cells in PC3 tumors that expressed costimulatory molecules MHC class II, CD40, CD80, and CD86 by 2- to 4-fold, providing further evidence that 2aG4 treatment drives the maturation of APCs (Fig. 4B). qRT-PCR and ELISA analyses showed that 2aG4 treatment of PC3 tumors shifted the balance of cytokines in the microenvironment from predominantly immunosuppressive (IL-10- and TGF-β–dominated) to predominantly immunostimulatory (IL-12-, TNF-α–dominated; Fig. 4C), further confirming the data shown in Fig. 3E. Taken together, these data indicate that 2aG4 treatment reactivates antitumor immunity at multiple levels.

Treatment with 2aG4 induces repolarization and activation of TAMs by binding to cell-surface phosphatidylserine in an Fc-dependent manner

A possible explanation for the large increase in M1:M2 ratio in 2aG4-treated tumors was that 2aG4 directly induces TAM repolarization. To test this, TAMs were isolated from PC3 tumors from untreated mice and incubated with 2aG4 *in vitro*. FACS analyses showed that TAMs cultured for 4 days in the presence of 2aG4 switched phenotype from predominantly M2-like ($F4/80^+$ and $Arg\text{-}1^+$) to predominantly M1-like ($F4/80^+$ and $iNOS^+$) that secreted NO (Fig. 5A and B). This effect was not seen with the $F(ab')_2$ fragment of 2aG4, indicating that the switch is dependent on Fcγ receptors. TAMs cultured in the presence of C44 did not switch phenotype. qRT-PCR analyses confirmed that TAMs cultured in the presence of 2aG4 had increased mRNA-encoding iNOS, inflammatory cytokines (IL-12 and TNF-α), and T-cell costimulatory molecules (CD80, CD86, and MHC class II) and decreased

Published OnlineFirst August 19, 2013; DOI: 10.1158/2326-6066.CIR-13-0073

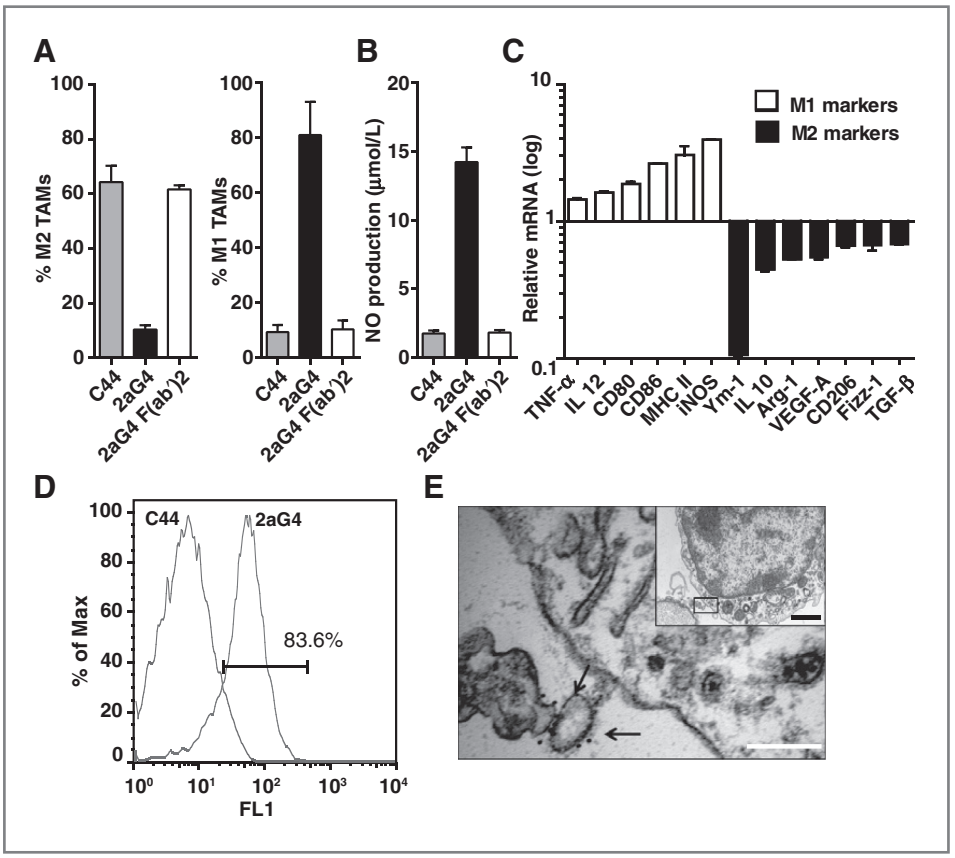

Figure 5. 2aG4 directly induces repolarization of TAMs by binding to phosphatidylserine on their cell surface and activating them in an Fc-dependent manner. A, FACS analyses showing that F4/80$^+$ TAMs from disaggregated PC3 tumors acquire an M1-like phenotype when cultured for 4 days with 2aG4. The M2-like (F4/80$^+$ and Arg-1$^+$) population and the M1-like (F4/80$^+$, iNOS$^+$) were quantified. The histograms show the percentages (mean ± SD) of double-positive cells. Statistically significant for 2aG4 versus C44 ($P < 0.0001$; Student two-tailed t test; three determinations). B, treatment of F4/80$^+$ TAMs with 2aG4 induces NO production (Griess reagent assay) in an Fc-dependent manner. Histograms, mean ± SD of triplicate determinations. C, qRT-PCR showing that F4/80$^+$ TAMs lose M2 markers and acquire M1 markers when cultured with 2aG4. The mRNA levels in 2aG4-treated cells are expressed relative to those in C44-treated cells. D, FACS analysis showing that F4/80$^+$ TAMs isolated from PC3 tumors have exposed phosphatidylserine. E, TEM of F4/80$^+$ TAM showing that phosphatidylserine on the cell surface is associated with the presence of phosphatidylserine-positive microvesicles. Size distribution of TAM-associated microvesicles: more than 300 microvesicles were measured. Forty-one percent were in the 100- to 200-nm size range (consistent with exosomes), 52% were in the 300- to 500-nm size range (possibly apoptotic microparticles), and 7% were more than 500 nm. The vesicles ranged in diameter from 100 to 500 nm and lacked the exosomal marker, Alix. Gold-labeled C44 did not bind (not shown). Arrows, gold-labeled 2aG4. Scale bars, black, 1,000 nm; white, 200 nm.

mRNA-encoding Arg-1, immunosuppressive cytokines (IL-10 and TGF-β), and VEGF-A (Fig. 5C).

We next determined whether TAMs have exposed phosphatidylserine. FACS analyses showed that freshly isolated TAMs from PC3 tumors bound to 2aG4 specifically (Fig. 5D). Electron microscopy studies revealed that 2aG4 does not bind directly to the plasma membrane of TAMs but to microvesicles attached to the cell surface (Fig. 5E). The microvesicles ranged in diameter from 100 to 500 nm, and they lacked the exosomal marker, Alix. Forty percent of the microvesicles carried one or more 2aG4-labeled gold particles. Control C44-labeled gold particles did not bind microvesicles or TAMs (data not shown).

Treatment with 2aG4 *in vitro* induces MDSCs differentiation into M1-like macrophages and dendritic cells

A possible explanation for the large decrease in MDSCs in 2aG4-treated tumors was that 2aG4 directly induces MDSC differentiation. To test this hypothesis, freshly isolated monocytic MDSCs from spleens of tumor-bearing mice were cultured with 2aG4, F(ab′)$_2$ fragment of 2aG4, or C44 control antibody for 5 days. 2aG4-treated monocytic MDSCs differentiated into macrophages and dendritic cells (Fig. 6A). After 5 days, only 10% of the 2aG4-treated MDSCs retained their MDSC phenotype (Gr-1$^+$ and CD11b$^+$) as compared with 60% of cells treated with C44 or F(ab′)$_2$ fragment of 2aG4. Fifty percent of cells in the 2aG4-treated cultures had a macrophage phenotype (CD11b$^+$ and F4/80$^+$) and 30% of cells had a dendritic cell phenotype (CD11b$^+$ and CD11c^{hi}; Fig. 6A). Neutrophils (F4/80$^-$, Gr-1$^+$, and CD11b^{Lo}) did not accumulate. Cells in 2aG4-treated cultures synthesized high levels of NO (Fig. 6B). These effects were not seen with cells cultured with the C44 antibody or the F(ab′)$_2$ fragment of 2aG4, indicating that the induction of differentiation is dependent on Fcγ receptors. Cells in 2aG4-treated cultures synthesized high levels of inflammatory cytokines, IL-6, TNF-α, and IL-12, but

Published OnlineFirst August 19, 2013; DOI: 10.1158/2326-6066.CIR-13-0073

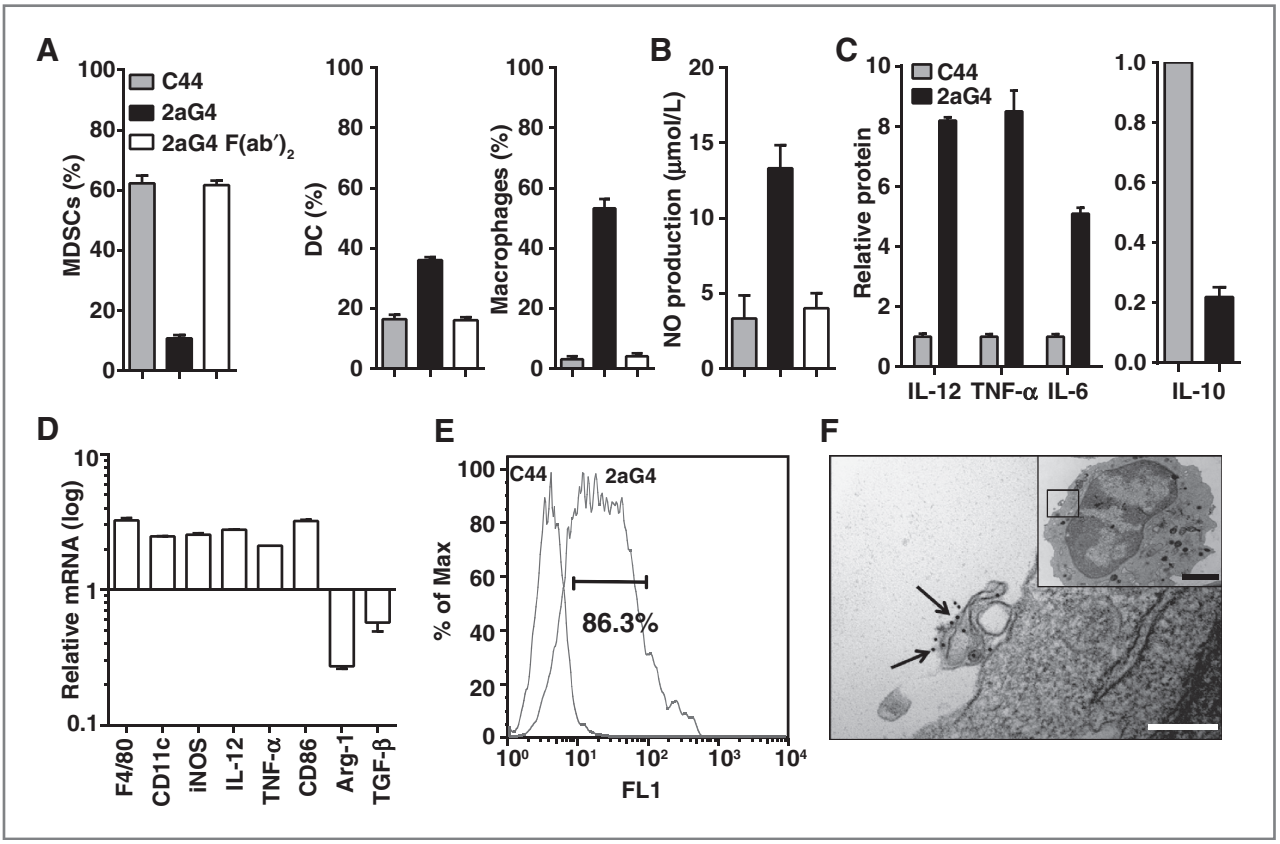

Figure 6. 2aG4 directly induces monocytic MDSCs to differentiate into dendritic cells and macrophages by binding to phosphatidylserine on their cell surface. A, FACS analyses showing that monocytic MDSCs (CD11b$^+$, Ly6G^{lo}, and Ly6C^{hi}) from the spleens of tumor-bearing mice differentiate into dendritic cells and macrophages when cultured for 4 days with 2aG4. MDSCs (CD11b$^+$ and Gr-1$^+$), macrophages (F4/80$^+$ and Gr-1$^-$), and dendritic cells (CDIIb$^+$, CD11c^{hi}, and Gr-1$^-$) were quantified by FACS. Histograms, mean percentage ± SD. Statistically significant for 2aG4 versus C44 ($P < 0.0001$; Student two-tailed t test; three determinations). B, treatment of monocytic MDSCs with 2aG4 induces NO production (Griess assay) in an Fc-dependent manner. Histograms, mean ± SD of triplicate determinations. C, ELISAs showing that 2aG4 treatment of monocytic MDSCs induces the production of inflammatory cytokines. D, qRT-PCR showing that 2aG4 treatment of monocytic MDSCs causes them to acquire markers of M1 macrophages and mature dendritic cells. The mRNA levels in 2aG4-treated cells are expressed relative to those in C44-treated cells. E, FACS analysis showing that monocytic MDSCs have exposed phosphatidylserine. F, TEM of a monocytic MDSC showing that phosphatidylserine on the cell surface is due to the presence of phosphatidylserine-positive microvesicles (100–500 nm diameter; Alix-). Arrows, gold-labeled 2aG4. Gold-labeled C44 did not bind (not shown). Scale bars, black, 1,000 nm; white, 200 nm.

low levels of IL-10, consistent with the phenotype of M1-like macrophages (Fig. 6C). In contrast, cells in C44-treated cultures synthesized low levels of inflammatory cytokines, IL-6, TNF-α, and IL-12, but high levels of IL-10, consistent with the phenotype of M2-like macrophages (Fig. 6C). qRT-PCR analyses confirmed that monocytic MDSCs cultured in the presence of 2aG4 had increased expression of mRNA-encoding macrophage marker (F4/80), dendritic cell marker (CD11c), iNOS, inflammatory cytokines (IL-12 and TNF-α), and T-cell costimulatory molecule (CD86), and decreased expression of mRNA-encoding Arg-1, and immunosuppressive cytokine (TGF-β; Fig. 6D). These findings indicate that 2aG4 promotes the differentiation of MDSCs into M1-like macrophages and dendritic cells.

We next determined whether monocytic MDSCs have exposed phosphatidylserine. FACS analyses showed that freshly isolated monocytic MDSCs from tumor-bearing mice bound to 2aG4 specifically (Fig. 6E). Electron microscopy studies revealed that 2aG4 does not bind directly to the plasma membrane of MDSCs but to the microvesicles attached to the cell surface (Fig. 6F).

Discussion

Recent evidence indicates that exposure of phosphatidylserine in the tumor microenvironment contributes to the immunosuppressed state of tumors (36, 43, 44). This suggests that the benefit of chemotherapy, radiotherapy, and other treatments that trigger tumor cell apoptosis is undermined by the increase in local tumor immunosuppression caused by phosphatidylserine exposed on dying tumor cells and their microvesicles (25, 43, 45). Here, we show that treatment of tumor-bearing mice with a phosphatidylserine-targeting antibody counteracts the tumor immunosuppression caused by chemotherapy and activates innate tumor immunity.

We show that 2aG4 functions at several levels to restore tumor immunity: (i) TAMs, which are predominantly in an

Published OnlineFirst August 19, 2013; DOI: 10.1158/2326-6066.CIR-13-0073

immunosuppressive M2-like state in untreated or docetaxel-treated tumors, become tumoricidal M1-like TAMs; (ii) highly immunosuppressive monocytic MDSCs in the tumor become depleted, whereas their M1-like TAM and dendritic cell progeny increases; and (iii) immature dendritic cells in tumors become mature and express T-cell costimulatary molecules, indicating their potential to function as APCs. It should be noted that as this study was carried out in immunodeficient animals, the impact of Tregs and other memory T cells on the phenotype-switch of the myeloid infiltrate cannot be assessed. However, our previous studies have shown that 2aG4 treatment allows dendritic cells to present tumor antigens and generate glioma-specific cytotoxic T cells in an immunocompetent rat glioma model (36). These results suggest that 2aG4 treatment reactivates both innate and adaptive tumor immunity.

The M1-like TAMs generated by 2aG4 treatment caused the destruction of tumor endothelium, vascular shutdown, and tumor cell death. M1-like TAMs were the only cell type observed in contact with intact and disintegrating vascular endothelium. Most likely, M1-like TAMs bind via activating Fcγ receptors to the antibody-coated endothelial cells and kill them by antibody-dependent cell-mediated cytotoxicity. Indeed, we have previously shown that macrophages lyse 2aG4-coated vascular endothelial cells in an Fc-dependent manner *in vitro* (36). 2aG4 does not mediate direct lysis of phosphatidylserine-expressing endothelial cells by complement (mouse or human). We attempted to deplete TAMs by systemic administration of liposomal clodronate but found, as have others (46), that TAMs were not depleted, most likely because of rapid liposome clearance by the liver and spleen. In addition to their vascular-damaging action, we show here that the M1-like TAMs synthesize NO and efficiently kill PC3 tumor cells *in vitro*, suggesting that they have direct tumoricidal activity *in vivo*.

One of the mechanisms by which 2aG4 induces TAM repolarization to an M1-like state is by binding to phosphatidylserine on the cell surface of TAM in an Fc-dependent manner. Our electron microscopy studies show that phosphatidylserine on the cell surface of TAM is due to the presence of phosphatidylserine-expressing microvesicles. It is likely that the phosphatidylserine-expressing microvesicles bind to phosphatidylserine receptors on the cell surface, sending signals that maintain TAMs in an anti-inflammatory M2-like state, similar to apoptotic cells (19–21). We hypothesize that 2aG4 binds to the microvesicles and ligates activating Fcγ receptors on the same cell or adjacent cells, sending signals that override the anti-inflammatory phosphatidylserine receptor signal and activate M1 differentiation (Fig. 7). The identity of the phosphatidylserine receptors on TAMs responsible for the anti-inflammatory signals is unknown, but it could be Tim3 (30). Tim4-positive cells have been observed to bind microvesicles (47). Thus, 2aG4 could also block the binding of phosphatidylserine-positive microvesicles to phosphatidylserine receptors on TAMs *in vivo*. Although we cannot rule out the possibility that M1 progenitors are recruited from the blood, our data indicate that repolarization of resident M2-TAMs is the primary mechanism.

The reduction in MDSCs and the overall increase in the number of TAMs and mature dendritic cells in 2aG4-treated tumors suggest that differentiation of MDSCs is also inhibited by phosphatidylserine-expressing microvesicles in the tumor

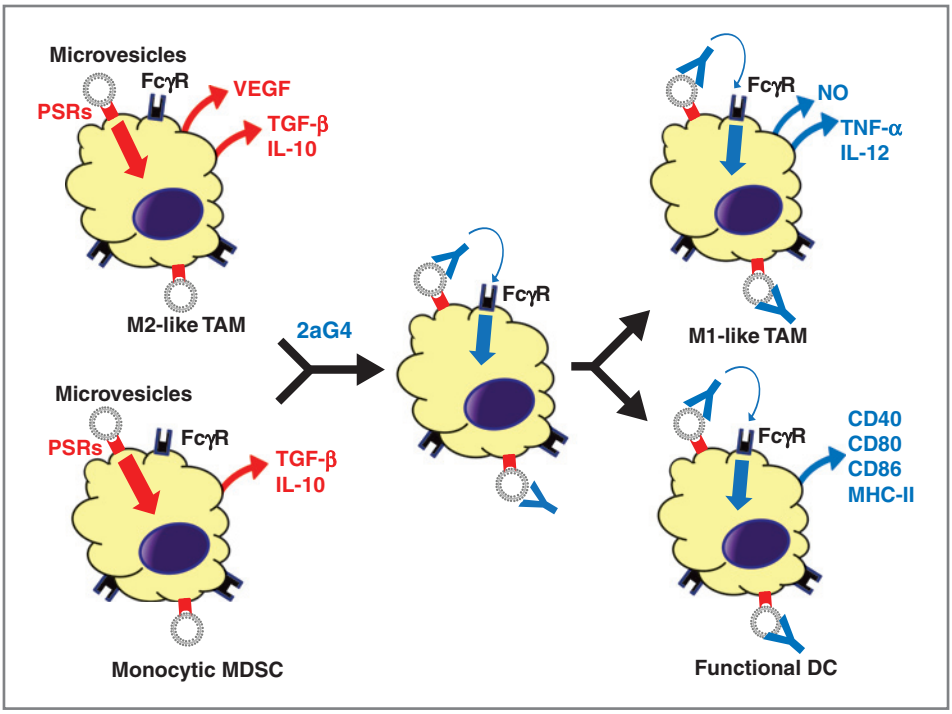

Figure 7. Hypothetical mechanism by which 2aG4 induces repolarization of TAMs and differentiation of monocytic MDSCs. Binding of phosphatidylserine-positive microvesicles to phosphatidylserine receptors (PSR) on TAMs signals them to adopt an immunosuppressive, proangiogenic M2-like state. 2aG4 binds to the microparticles and ligates FcγRs, sending activating signals that induce the TAMs to repolarize into their immunostimulatory, NO-secreting, tumoricidal M1-like state. Binding of phosphatidylserine-positive microvesicles to PSRs on monocytic MDSCs retards their differentiation, keeping them in an immunosuppressive state. 2aG4 binds to the microvesicles and ligates FcγRs sending activating signals that induce differentiation into M1-like TAMs and dendritic cells.

Published OnlineFirst August 19, 2013; DOI: 10.1158/2326-6066.CIR-13-0073

microenvironment. We speculate that 2aG4 binds to and stimulates MDSCs differentiation into TAMs and dendritic cells. We isolated monocytic MDSCs ($CD11b^+$, $Ly6G^{lo}$, and $Ly6C^{hi}$) from the spleens of tumor-bearing mice (48), and cultured them with 2aG4 in the absence of additional growth factors. We found that 2aG4 treatment *in vitro* induces the differentiation of monocytic MDSCs into M1-like macrophages and dendritic cells (Fig. 6). These progeny secreted NO and their cytokine profile switched from immunosuppressive to immunostimulatory. Electron microscopy studies confirmed that MDSCs, like TAMs, are phosphatidylserine-positive due to the presence of phosphatidylserine-expressing microvesicles on their surface (Fig. 6). It is likely that dendritic cells are also prevented from maturing in tumors by the exposed phosphatidylserine, as dendritic cells have exposed phosphatidylserine and annexin 5A facilitates dendritic cell maturation *in vitro* (49). 2aG4 may stimulate dendritic cell maturation in tumors by a mechanism analogous to that shown in Fig. 7.

Bavituximab, the human chimeric version of 2aG4, in combination with chemotherapy, is being used to treat patients with cancer in randomized clinical trials (38–40). Impressive antitumor effects in patients with cancer have been obtained with other antibodies that enhance tumor immunity, including anti-PD1, anti-PD-1L, and ipilimumab (anti-CTLA-4; ref. 50). Unlike these antibodies, which inhibit negative feedback pathways in immune cell activation, bavituximab seems to act by reversing the immunosuppressive effects of exposed phosphatidylserine in the tumor microenvironment, resulting in activation of local tumor immunity and damage to tumor vasculature.

Disclosure of Potential Conflicts of Interest

X. Huang and P.E. Thorpe are consultant/advisory board members of Peregrine Pharmaceuticals, Inc. No potential conflicts of interest were disclosed by the other authors.

Authors' Contributions

Conception and design: Y. Yin, X. Huang, K.D. Lynn, P.E. Thorpe
Development of methodology: Y. Yin, X. Huang, P.E. Thorpe
Acquisition of data (provided animals, acquired and managed patients, provided facilities, etc.): Y. Yin, X. Huang, K.D. Lynn, P.E. Thorpe
Analysis and interpretation of data (e.g., statistical analysis, biostatistics, computational analysis): Y. Yin, X. Huang, K.D. Lynn, P.E. Thorpe
Writing, review, and/or revision of the manuscript: Y. Yin, X. Huang, K.D. Lynn, P.E. Thorpe
Administrative, technical, or material support (i.e., reporting or organizing data, constructing databases): X. Huang, P.E. Thorpe
Study supervision: X. Huang, P.E. Thorpe

Acknowledgments

The authors thank Dan Ye, Shuzhen Li, and Janie Iglehart for technical assistance and Drs. Alan Schroit, E. Sally Ward, and Rolf A. Brekken for discussions and comments on the article.

Grant Support

This work was supported by a sponsored research agreement with Peregrine Pharmaceuticals, Inc., Department of Defense grants PC05031 (to P.E. Thorpe) and PC080475 (to Y. Yin), an NIH-supported Small Animal Imaging Research Program at University of Texas Southwestern (U24CA126608), and the Gillson Longenbaugh Foundation.

The costs of publication of this article were defrayed in part by the payment of page charges. This article must therefore be hereby marked *advertisement* in accordance with 18 U.S.C. Section 1734 solely to indicate this fact.

Received June 9, 2013; revised August 6, 2013; accepted August 10, 2013; published OnlineFirst August 19, 2013.

References

1. Gabrilovich D. Mechanisms and functional significance of tumour-induced dendritic-cell defects. Nat Rev Immunol 2004;4:941–52.
2. Gabrilovich DI, Nagaraj S. Myeloid-derived suppressor cells as regulators of the immune system. Nat Rev Immunol 2009;9:162–74.
3. Yang R, Cai Z, Zhang Y, Yutzy WH IV, Roby KF, Roden RB. CD80 in immune suppression by mouse ovarian carcinoma-associated Gr-1^+CD11b^+ myeloid cells. Cancer Res 2006;66:6807–15.
4. Huang B, Pan PY, Li Q, Sato AI, Levy DE, Bromberg J, et al. Gr-1^+CD115^+ immature myeloid suppressor cells mediate the development of tumor-induced T regulatory cells and T-cell anergy in tumor-bearing host. Cancer Res 2006;66:1123–31.
5. Li H, Han Y, Guo Q, Zhang M, Cao X. Cancer-expanded myeloid-derived suppressor cells induce anergy of NK cells through membrane-bound TGF-beta 1. J Immunol 2009;182:240–9.
6. Balkwill F, Mantovani A. Inflammation and cancer: back to Virchow? Lancet 2001;357:539–45.
7. Bronte V, Apolloni E, Cabrelle A, Ronca R, Serafini P, Zamboni P, et al. Identification of a CD11b(+)/Gr-1(+)/CD31(+) myeloid progenitor capable of activating or suppressing CD8(+) T cells. Blood 2000;96:3838–46.
8. Filipazzi P, Valenti R, Huber V, Pilla L, Canese P, Iero M, et al. Identification of a new subset of myeloid suppressor cells in peripheral blood of melanoma patients with modulation by a granulocyte-macrophage colony-stimulation factor-based antitumor vaccine. J Clin Oncol 2007;25:2546–53.
9. Corzo CA, Condamine T, Lu L, Cotter MJ, Youn JI, Cheng P, et al. HIF-1alpha regulates function and differentiation of myeloid-derived suppressor cells in the tumor microenvironment. J Exp Med 2010;207:2439–53.
10. Kusmartsev S, Gabrilovich DI. Inhibition of myeloid cell differentiation in cancer: the role of reactive oxygen species. J Leukoc Biol 2003;74:186–96.
11. Kusmartsev S, Gabrilovich DI. STAT1 signaling regulates tumor-associated macrophage-mediated T cell deletion. J Immunol 2005;174:4880–91.
12. Troy A, Davidson P, Atkinson C, Hart D. Phenotypic characterisation of the dendritic cell infiltrate in prostate cancer. J Urol 1998;160:214–9.
13. Murdoch C, Muthana M, Coffelt SB, Lewis CE. The role of myeloid cells in the promotion of tumour angiogenesis. Nat Rev Cancer 2008;8:618–31.
14. Mantovani A, Sozzani S, Locati M, Allavena P, Sica A. Macrophage polarization: tumor-associated macrophages as a paradigm for polarized M2 mononuclear phagocytes. Trends Immunol 2002;23:549–55.
15. Murdoch C, Lewis CE. Macrophage migration and gene expression in response to tumor hypoxia. Int J Cancer 2005;117:701–8.
16. Kurahara H, Shinchi H, Mataki Y, Maemura K, Noma H, Kubo F, et al. Significance of M2-polarized tumor-associated macrophage in pancreatic cancer. J Surg Res 2011;167:e211–9.
17. Yoshikawa K, Mitsunaga S, Kinoshita T, Konishi M, Takahashi S, Gotohda N, et al. Impact of tumor-associated macrophages on invasive ductal carcinoma of the pancreas head. Cancer Sci 2012;103:2012–20.
18. Ma J, Liu L, Che G, Yu N, Dai F, You Z. The M1 form of tumor-associated macrophages in non–small cell lung cancer is positively associated with survival time. BMC Cancer 2010;10:112.
19. Fadok VA, Bratton DL, Konowal A, Freed PW, Westcott JY, Henson PM. Macrophages that have ingested apoptotic cells *in vitro* inhibit proinflammatory cytokine production through autocrine/paracrine

Published OnlineFirst August 19, 2013; DOI: 10.1158/2326-6066.CIR-13-0073

mechanisms involving TGF-beta, PGE2, and PAF. J Clin Invest 1998; 101:890–8.
20. Fadok VA, Voelker DR, Campbell PA, Cohen JJ, Bratton DL, Henson PM. Exposure of phosphatidylserine on the surface of apoptotic lymphocytes triggers specific recognition and removal by macrophages. J Immunol 1992;148:2207–16.
21. McDonald PP, Fadok VA, Bratton D, Henson PM. Transcriptional and translational regulation of inflammatory mediator production by endogenous TGF-beta in macrophages that have ingested apoptotic cells. J Immunol 1999;163:6164–72.
22. Balasubramanian K, Schroit AJ. Aminophospholipid asymmetry: a matter of life and death. Annu Rev Physiol 2003;65:701–34.
23. Ran S, Downes A, Thorpe PE. Increased exposure of anionic phospholipids on the surface of tumor blood vessels. Cancer Res 2002;62:6132–40.
24. Ran S, He J, Huang X, Soares M, Scothorn D, Thorpe PE. Antitumor effects of a monoclonal antibody that binds anionic phospholipids on the surface of tumor blood vessels in mice. Clin Cancer Res 2005; 11:1551–62.
25. Taylor DD, Gercel-Taylor C. Exosomes/microvesicles: mediators of cancer-associated immunosuppressive microenvironments. Semin Immunopathol 2011;33:441–54.
26. Utsugi T, Schroit AJ, Connor J, Bucana CD, Fidler IJ. Elevated expression of phosphatidylserine in the outer membrane leaflet of human tumor cells and recognition by activated human blood monocytes. Cancer Res 1991;51:3062–6.
27. He J, Luster TA, Thorpe PE. Radiation-enhanced vascular targeting of human lung cancers in mice with a monoclonal antibody that binds anionic phospholipids. Clin Cancer Res 2007;13:5211–8.
28. Huang X, Bennett M, Thorpe PE. A monoclonal antibody that binds anionic phospholipids on tumor blood vessels enhances the antitumor effect of docetaxel on human breast tumors in mice. Cancer Res 2005;65:4408–16.
29. He M, Kubo H, Morimoto K, Fujino N, Suzuki T, Takahasi T, et al. Receptor for advanced glycation end products binds to phosphatidylserine and assists in the clearance of apoptotic cells. EMBO Rep 2011;12:358–64.
30. Freeman GJ, Casasnovas JM, Umetsu DT, DeKruyff RH. TIM genes: a family of cell surface phosphatidylserine receptors that regulate innate and adaptive immunity. Immunol Rev 2010;235:172–89.
31. Park D, Tosello-Trampont AC, Elliott MR, Lu M, Haney LB, Ma Z, et al. BAI1 is an engulfment receptor for apoptotic cells upstream of the ELMO/Dock180/Rac module. Nature 2007;450:430–4.
32. Park SY, Jung MY, Kim HJ, Lee SJ, Kim SY, Lee BH, et al. Rapid cell corpse clearance by stabilin-2, a membrane phosphatidylserine receptor. Cell Death Differ 2008;15:192–201.
33. Balasubramanian K, Schroit AJ. Characterization of phosphatidylserine-dependent beta2-glycoprotein I macrophage interactions. Implications for apoptotic cell clearance by phagocytes. J Biol Chem 1998;273:29272–7.
34. Hanayama R, Tanaka M, Miyasaka K, Aozasa K, Koike M, Uchiyama Y, et al. Autoimmune disease and impaired uptake of apoptotic cells in MFG-E8–deficient mice. Science 2004;304:1147–50.
35. Bondanza A, Zimmermann VS, Rovere-Querini P, Turnay J, Dumitriu IE, Stach CM, et al. Inhibition of phosphatidylserine recognition heightens the immunogenicity of irradiated lymphoma cells *in vivo*. J Exp Med 2004;200:1157–65.
36. He J, Yin Y, Luster TA, Watkins L, Thorpe PE. Antiphosphatidylserine antibody combined with irradiation damages tumor blood vessels and induces tumor immunity in a rat model of glioblastoma. Clin Cancer Res 2009;15:6871–80.
37. Kenis H, Reutelingsperger C. Targeting phosphatidylserine in anticancer therapy. Curr Pharm Des 2009;15:2719–23.
38. Digumarti R, Suresh AV, Bhattacharyya GS, Dasappa L, Shan J. Phase II study of bavituximab plus paclitaxel and carboplatin in untreated locally advanced or metastatic non–small cell lung cancer: interim results. J Clin Oncol 2010;28:15s, 7589.
39. Gerber DE, Stopeck AT, Wong L, Rosen LS, Thorpe PE, Shan JS, et al. Phase I safety and pharmacokinetic study of bavituximab, a chimeric phosphatidylserine-targeting monoclonal antibody, in patients with advanced solid tumors. Clin Cancer Res 2011;17: 6888–96.
40. Jain M, Raizada N, Kuttan R, Shan J, Digumarti R. Phase II study of bavituximab plus paclitaxel and carboplatin in locally advanced or metastatic breast cancer: interim results. J Clin Oncol 2010;28:15s, 1062.
41. Luster TA, He J, Huang X, Maiti SN, Schroit AJ, de Groot PG, et al. Plasma protein beta-2-glycoprotein 1 mediates interaction between the anti-tumor monoclonal antibody 3G4 and anionic phospholipids on endothelial cells. J Biol Chem 2006;281:29863–71.
42. Ran S, Thorpe PE. Phosphatidylserine is a marker of tumor vasculature and a potential target for cancer imaging and therapy. Int J Radiat Oncol Biol Phys 2002;54:1479–84.
43. Szajnik M, Czystowska M, Szczepanski MJ, Mandapathil M, Whiteside TL. Tumor-derived microvesicles induce, expand and up-regulate biological activities of human regulatory T cells (Treg). PLoS ONE 2010;5:e11469.
44. Yan X, Doffek K, Yin C, Krein M, Phillips M, Sugg SL, et al. Annexin-V promotes anti-tumor immunity and inhibits neuroblastoma growth *in vivo*. Cancer Immunol Immunother 2012;61:1917–27.
45. Lima LG, Chammas R, Monteiro RQ, Moreira ME, Barcinski MA. Tumor-derived microvesicles modulate the establishment of metastatic melanoma in a phosphatidylserine-dependent manner. Cancer Lett 2009;283:168–75.
46. Beatty GL, Chiorean EG, Fishman MP, Saboury B, Teitelbaum UR, Sun W, et al. CD40 agonists alter tumor stroma and show efficacy against pancreatic carcinoma in mice and humans. Science 2011;331:1612–6.
47. Miyanishi M, Tada K, Koike M, Uchiyama Y, Kitamura T, Nagata S. Identification of Tim4 as a phosphatidylserine receptor. Nature 2007; 450:435–9.
48. Zhou J, Wu J, Chen X, Fortenbery N, Eksioglu E, Kodumudi KN, et al. Icariin and its derivative, ICT, exert anti-inflammatory, anti-tumor effects, and modulate myeloid derived suppressive cells (MDSCs) functions. Int Immunopharmacol 2011;11:890–8.
49. Chen X, Doffek K, Sugg SL, Shilyansky J. Phosphatidylserine regulates the maturation of human dendritic cells. J Immunol 2004; 173:2985–94.
50. Simeone E, Ascierto PA. Immunomodulating antibodies in the treatment of metastatic melanoma: the experience with anti-CTLA-4, anti-CD137, and anti-PD1. J Immunotoxicol 2012;9:241–7.

Supplementary Figure Legends

Supplementary Fig. S1. **Regression of large subcutaneous LNCaP tumors and prevention of relapse from castration-resistant disease in mice treated with castration combined with 2aG4 plus docetaxel**. Mice bearing 1 cm diameter subcutaneous LNCaP tumors were sham-castrated (**A**) or castrated (**B**) and treated twice weekly thereafter with C44 (black ●), 2aG4 (red ▲), docetaxel (green ▼), or 2aG4 plus docetaxel (blue ■). Doses of antibody were 4 mg/kg and docetaxel was 5 mg/kg, both i.p. All animals received human β2GP1 (4 mg/kg, i.p) with each treatment to enable binding of 2aG4 to PS. Left panels: Tumor volume over time; Right panels: Tumor weight at the end of the experiment. Points and lines, mean tumor volume (n = 10); bars, s.e.m. *Significant for 2aG4 or docetaxel versus C44 ($P<0.0001$); **Significant for combination versus 2aG4 or docetaxel alone ($P\leq0.05$) (ANOVA followed by Tukey's range test).

Supplementary Fig. S2. Damage to tumor vasculature in LNCaP tumors induced by treatment with 2aG4. (**A**) Exposure of PS on tumor endothelium and amplification by docetaxel. Upper panels show representative sections from LNCaP tumor-bearing mice that had been injected with saline (left) or docetaxel (10mg/kg, i.p, right) followed 48 h later by bavituximab to detect PS or rituximab (control). Sections were stained for bavituximab (green), CD31 (red) and nuclei (DAPI, blue) and images merged. Arrows indicate bavituximab-stained vessels. The percentage of the CD31-positive area of

sections that co-stained for PS reached a maximum 48 h after injection of docetaxel (histograms). (**B**) Denudation of vascular endothelium in LNCaP tumors in mice treated with 2aG4. The merged image (lower right) shows stripped vessels, as identified by collagen IV staining (green) and absence of endothelium (CD31, red). (**C**) Reduction of tumor vascularity (vessels/0.079 mm^2) and perfusion (% area stained by Hoescht 33342 dye) in LNCaP tumor-bearing mice treated with 2aG4 alone or in combination with docetaxel. In **A, C, D**, 5 animals per group were analyzed. Histograms are means ± s.d. Number of determinations (n) were 120-150 (**A**), 50 (**C**). *Significant for 2aG4 versus C44 control ($P<0.0001$); **Significant for 2aG4 plus docetaxel versus 2aG4 alone ($P<0.05$) (Student's two-tailed t-test). Scale bars, 100 μm.

Supplementary Fig. S3. ***TAMs in LNCaP tumors switch polarity from an M2-like phenotype to an M1-like phenotype after 2aG4 treatment.*** *(**A**)* Representative frozen sections showing that the TAMs that destroy tumor vasculature in 2aG4-treated mice are of M1-like phenotype, whereas the TAMs in C44-treated mice are of M2-like phenotype. Tumor sections were stained for TAMs (F4/80, green), iNOS (blue, upper left center panels), Arg-1 (blue, lower left center panels) or (vascular endothelium (CD31, red). In 2aG4-treated mice, almost all the TAMs congregating around damaged vessels (arrows) costained for F4/80 and iNOS (light blue in merged image) showing they were of M1-like phenotype. Other cell types (NK, granulocytes, DCs) were not present in the packs of cells around damaged vessels (not shown). In C44-treated mice, almost all the TAMs costained for F4/80 and Arg-1 (light blue in merged image), showing they were of M2-like phenotype. The M2-like TAMs were scattered throughout

the tumor interstitium and were not associated with the vessels. Scale bars, 100 μm. (**B**) A large increase in M1:M2 ratio in TAMs is caused by 2aG4 treatment. Histograms show the area of LNCaP tumor sections occupied by M1 (F4/80+, iNOS+) or M2 (F4/80+, Arg-1+) TAMs, and the calculated M1:M2 ratio. Bars, mean percentage areas ± s.d. Number of determinations, 40-60. Differences between 2aG4 and C44 are significant ($P<0.0001$, Student's two tailed t-test).

Supplementary Fig. S4. 2aG4 treatment of LNCaP tumor-bearing mice decreases MDSCs, increases TAMs and mature DCs. (**A**) Representative frozen sections of subcutaneous LNCaP tumors showing that 2aG4 treatment of the mice decreases the presence of MDSCs and increases the presence of TAMs and mature DCs. Upper panels, C44-treated control mice; lower panels, 2aG4-treated mice. The sections were stained for MDSCs (CD11b+, Gr-1+), TAMs (F4/80+), mature DCs ($CD11c^{hi}$, $CD86^{hi}$), and nuclei (DAPI, blue). MDSCs (left) and mature DCs (right) appear yellow in the merged images. TAMs in the central panels appear green. Scale bar, 100 μm. (**B**) Histograms showing the mean percentage area ± s.d. of tumor sections occupied by the cells. Differences between 2aG4 and C44 are significant ($P<0.0001$, $n=40$, Student's two-tailed t-test).

Supplementary figure S1

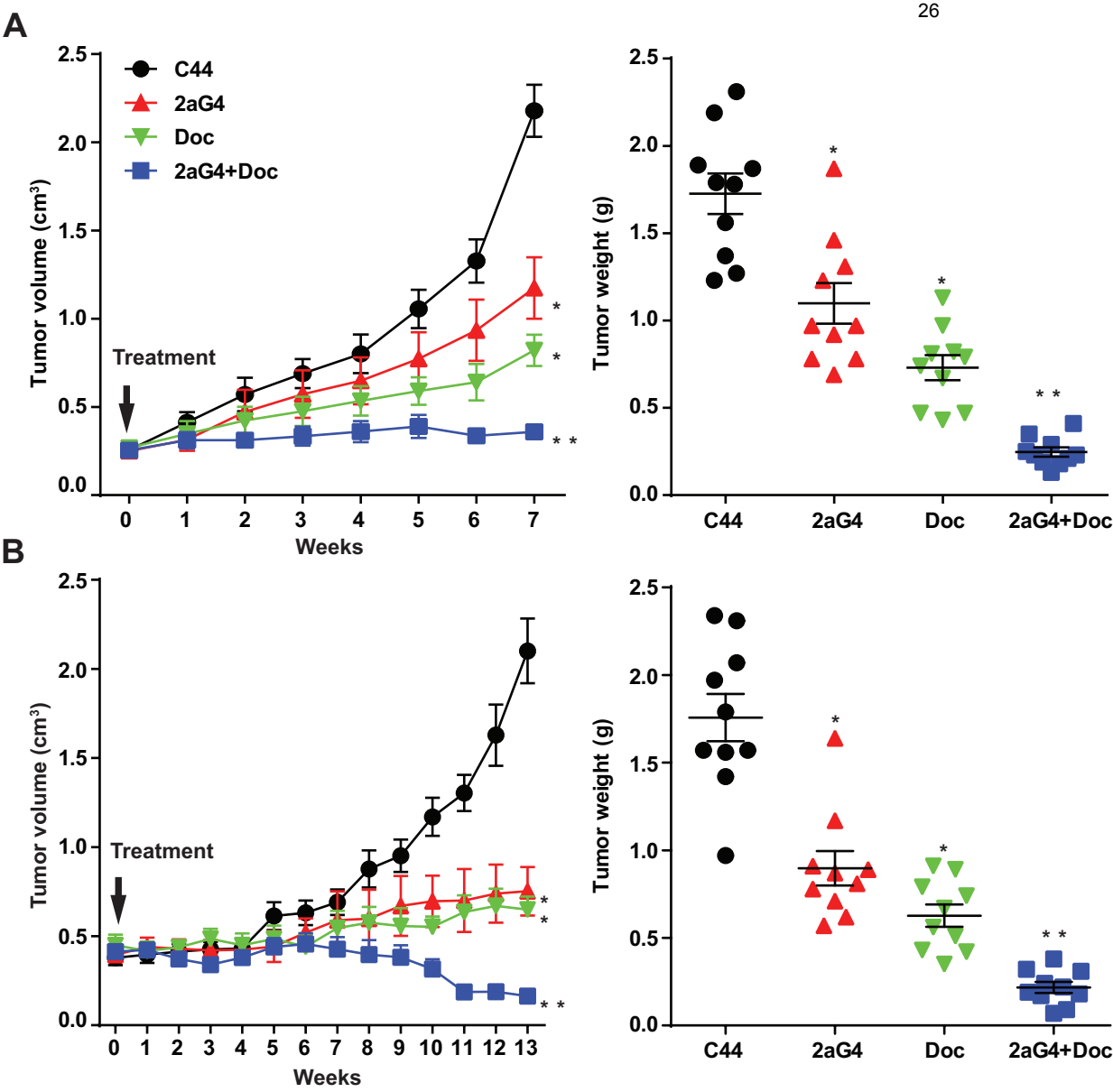

Supplementary figure S2

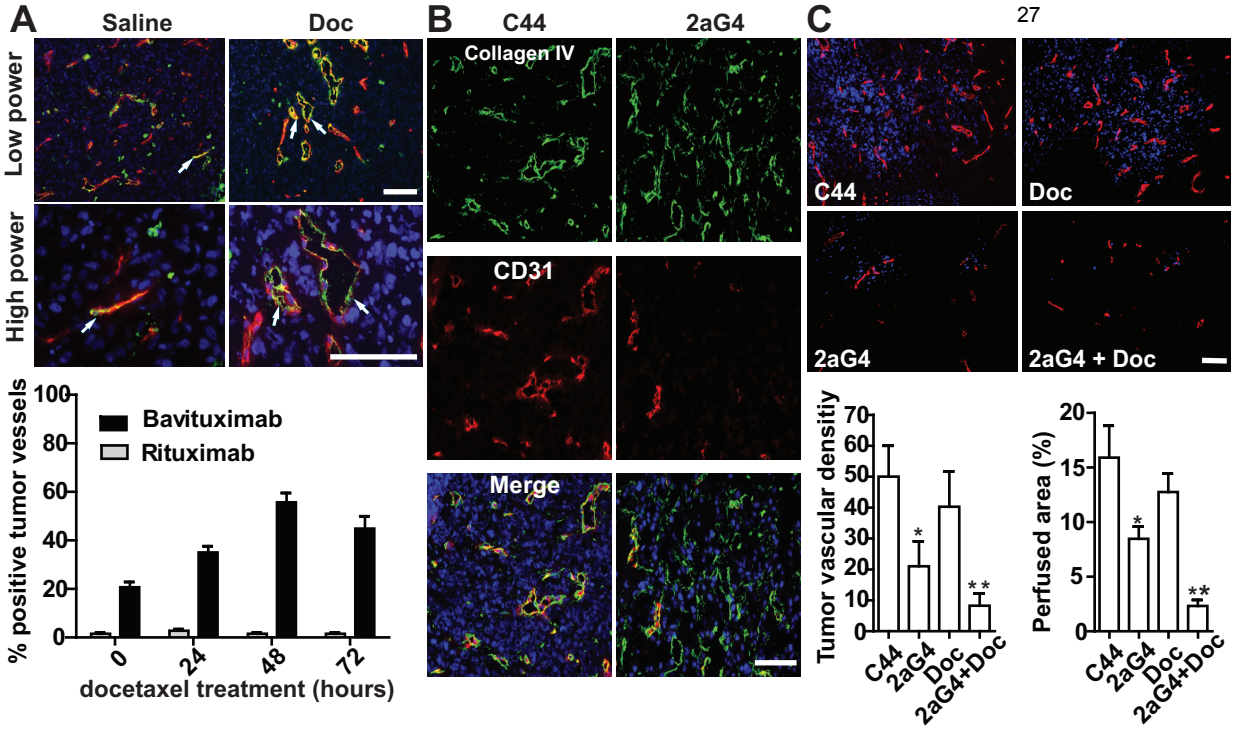

Supplementary figure S3

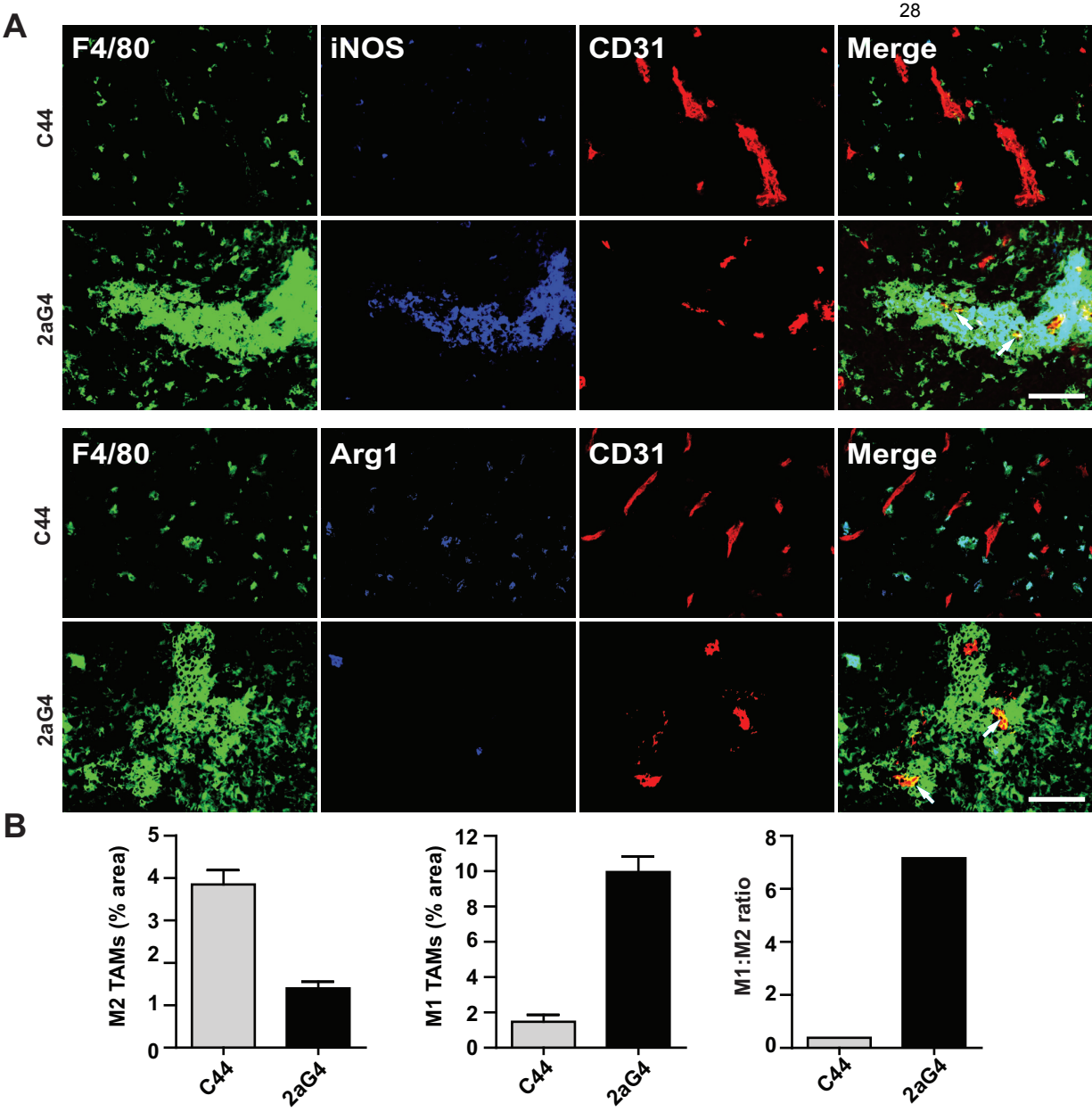

Supplementary figure S4